JOURNAL OF COMPUTATIONAL PHYSICS 85, 342–389 (1989)

A Boundary Integral Approach to Unstable Solidification*

JOHN STRAIN†

Department of Mathematics and Lawrence Berkeley Laboratory, University of California, Berkeley, California 94720

Received August 23, 1988

We consider the supercooled Stefan problem with a general anisotropic curvature- and velocity-dependent boundary condition on the moving interface. We present numerical methods, based on an integral equation formulation and including a new algorithm for moving curves with curvature-dependent velocity. These methods compute a periodic interface with $O(\Delta t)$ accuracy, where Δt is the time step. Previous work has been limited to short time spans and achieved slightly less than $O(\Delta t^{1/2})$ accuracy. Accurate numerical results are seen to agree with the predictions of linear stability theory. This agreement has eluded previous authors, because their numerical methods suffered from grid effects and their linear stability theory was incorrect. We study the long-time evolution of an unstable interface. Our computations exhibit the beginnings of a sidebranching instability when the boundary condition includes anisotropy and tip-splitting in the isotropic case.

INTRODUCTION

Recently, there has been much interest in the supercooled Stefan problem with a curvature-dependent boundary condition on the phase interface, as a model for the spontaneous pattern formation believed to occur in dendritic solidification of a pure substance from an undercooled melt. This *symmetric model* was introduced in the metallurgical and physical literature [29, 36, 42]; some recent works propose and study more general boundary conditions [6, 26].

Most of the physical literature has studied the problem using asymptotic analysis, and applied numerical methods only to solve various approximate equations [2, 36]. Numerical methods have been successfully applied to steady-state equations [40, 46] and to equations for smoothed interfaces [7, 19]. Only a few authors have attempted to solve the full time-dependent problem [10, 48, 52], and it seems that none have computed the interface accurately in the nonlinear regime, where interesting phenomena like sidebranching [29], tip-splitting [43], and formation of cellular fronts [36] are presumed to occur. Even for small perturbations of simple

* This work was supported by a NSF Graduate Fellowship, an IBM Predoctoral Fellowship, and by the Applied Mathematical Sciences subprogram of the Office of Energy Research U.S. Department of Energy under Contract DE-AC03-76SF00098.

† Current address: Courant Institute, 251 Mercer Street, New York, NY 10012.

0021-9991/89 $3.00

shapes evolving for short times, no quantitative agreement with linear stability theory has been demonstrated.

In this paper, we present a numerical method for solving the supercooled Stefan problem in two space dimensions, with a general anisotropic curvature- and velocity-dependent temperature boundary condition on the phase interface. Our method is based on eliminating the temperature field and computing only the interface. There are two difficulties in this approach; first, computing the velocity requires solution of a nonlinear history-dependent singular integral equation on the moving boundary; second, moving a curve with curvature-dependent velocity is difficult even if the velocity is a simple function of curvature [47]. The first difficulty is easiest to understand in the simple case when the interface is the graph of a function: its resolution involves several new ideas. The second difficulty is resolved by a reformulation of the curve motion problem and a new numerical algorithm for solving the reformulated problem.

Our method computes the interface with $O(\Delta t)$ accuracy, where Δt is the time step. This compares favorably with previous approaches, which achieve less than $O(\Delta t^{1/2})$ accuracy, even for the simpler curvature-independent classical Stefan problem without supercooling. Our accurate numerical results agree with linear stability theory; such agreement has eluded previous authors. Previous authors were unable to obtain agreement between numerical results and linear stability theory because most numerical results suffer from grid effects (to be explained later) and because the linear stability theory with which they compared their results is not quantitatively accurate. We also use our method to carry out several long-time computations in which physically interesting phenomena occur.

In Section 1, we review some previous theoretical and numerical work on this and related problems, and give references to derivations from nonequilibrium thermodynamics. Then we reformulate the moving boundary problem as a nonlinear history-dependent singular integral equation for the normal velocity of the interface.

Section 2 contains a numerical method for computing the interface while it remains the graph $\{x = s,\ y = y(t, s) \mid -\infty < s < \infty\}$ of a 2π-periodic function $y(t, s)$. We deal with this simple case first because it allows us to learn how to solve the integral equation for the velocity, without worrying about how to move the curve. Of course, the boundary does not remain a graph forever, so this method is useful only for moderate time spans and moderate deformations of a flat interface. However, moderate time spans suffice to check agreement with linear stability theory. We also show experimentally that the numerical method is first-order accurate.

Section 3 contains a numerical method for computing a general interface, no longer restricted to graphs. This includes a reformulation of the general problem of moving curves, as an evolution equation for the normal angle ϕ. Using this equation to move the boundary and computing the velocity V from the integral equation results in a complicated but reliable numerical method, which is first-order accurate and stable. We solve an additional ordinary differential equation to keep

track of arclength, and we introduce an algorithm which keeps points equally spaced on the curve without resdistribution.

Our results show that the principle of computing only the moving boundary leads to an effective and accurate numerical method. Our computations exhibit sidebranching only when the boundary condition includes anisotropy, as predicted in [37]; we see a well-developed tip-splitting instability in the isotropic case.

This paper is based on part of the author's doctoral dissertation, "Numerical study of dendritic solidification," written at the Department of Mathematics, University of California at Berkeley, under the supervision of Alexandre Chorin.

1. Some Previous Work

1.1. *Physics*

Consider, for the sake of comparison with our problem, the melting of ice in water. This is a smooth, stable phenomenon, modeled by the classical two-phase Stefan problem: The temperature field u satisfies the heat equation

$$\partial_t u = \Delta u$$

in each phase (water or ice) separately, the normal velocity is the jump in the normal component of heat flux,

$$V = -[\partial u/\partial v],$$

across the interface, and the temperature on the interface is the equilibrium melting temperature; by a shift of origin in the temperature scale, $u = 0$ on the interface. The notation is explained in Section 2. With appropriate initial and boundary conditions for u, this is a fairly well-understood and mathematically well-posed problem, for which many results of existence, uniqueness, and regularity have been proven. Many of the more recent results [5] rely on the weak formulation introduced by Duvaut [15] and the theory of variational inequalities [35], but earlier work was done with integral equations, maximum principles, and other tools from the classical theory of partial differential equations [20, 45].

In the physical situations with which we will be concerned, on the other hand, it often happens that the liquid phase is supercooled; $u < 0$ in the liquid phase. In practice, water can be cooled substantially below 0°C without freezing, if there is no "seed" to start the freezing process. A small disturbance can then begin a rapid and unstable change of phase, *dendritic solidification.* The large-scale shape of the resulting solid—for example, the diameter of a snowflake—is typically a reproducible function of a few physical parameters, but the detailed small-scale structure has a complex but organized appearance. Currently many workers [11, 37, 36, 33, 43, 2, 46] are interested in this problem of *pattern formation.*

Supercooling of the liquid phase requires a re-examination of the assumptions and formulation of the classical Stefan problem. Classically, the water is the set

where $u > 0$, the ice is the set where $u < 0$, and the interface is the set where $u = 0$. When supercooling is present, however, a snapshot of the temperature field at any given time does not determine the interface, because u can be negative in either phase. Thus the only way we can keep track of the interface is by following it continuously in time. This requires that the interface itself *move* smoothly in time. Physically, this means that liquid can solidify only adjacent to preexisting solid.

Unfortunately, both linear stability analysis [50, 36, 42, 44] and rigorous theory [3] show that the interface does not remain smooth when the liquid is supercooled. Linear stability theory gives a growth exponent $\gamma(k) = V|k|$, where V is the velocity of the underlying flat interface and k is the wavenumber of the perturbation; disturbances to a flat interface grow like $e^{t\gamma(k)}$, with small wavelengths growing faster, so the interfacial structure becomes very complicated. Since a real snowflake, for example, exhibits a complicated structure only down to a certain length scale, below which the interface is microscopically smooth, this indicates that supercooled solidification is not well modelled by the classical Stefan problem. Furthermore, an analysis of the classical Stefan problem by Di Benedetto and Friedman shows that finite-time blowup occurs when the water is supercooled [3]. Hence modification of the classical Stefan problem is necessary, if we are to model supercooling of the liquid phase.

The various modified models proposed usually differ from the classical Stefan problem only in the boundary condition $u = 0$ on the moving boundary; exceptions, however, are [56, 59]. The most classical models include surface tension to assign the interface an energy proportional to its area and result in a curvature-dependent "Gibbs–Thomson relation"

$$u = -\varepsilon_C C \tag{1}$$

on the interface. Here ε_C is a small constant and C is the curvature of the interface, taken to be positive where the center of the osculating circle lies in the solid phase. More recently, several authors [26, 6] have proposed anisotropic curvature- and velocity-dependent boundary conditions of the form

$$u = -\varepsilon_C(\phi) C - \varepsilon_V(\phi) V, \tag{2}$$

where ϕ is the angle between the normal to the interface and a fixed axis and V is the normal velocity. Typically,

$$\varepsilon_C(\phi) = \varepsilon_C(1 - A \cos k_A \phi)$$
$$\varepsilon_V(\phi) = \varepsilon_V(1 - A \cos k_A \phi),$$

where $A \in [0, 1)$ is the coefficient of anisotropy and k_A is a small integer connected with the crystalline anisotropy of the solidifying substance. These relations involve the non-equilibrium concept of velocity and therefore cannot follow from equilibrium thermodynamics, unlike the curvature-dependent (but velocity-independent and isotropic) Gibbs–Thomson relation (1).

There are three theoretical frameworks within which the general boundary condition (2) can be derived; the phase field model of phase transitions [6], Cahn–Hilliard theory [8], and thermodynamics with interfacial energy and entropy [26]. The first two approaches work with smoothed interfaces and microscopic models, extracting (2) in a singular limit; the last attempts to include sharp interfaces in thermodynamics.

1.2. *Existence Theory*

No rigorous existence and uniqueness results are known for the supercooled Stefan problem with the curvature-dependent boundary conditions (1.1.1) or (1.1.2). We describe, however, a local existence and uniqueness result for a simpler model problem, because it suggests the curve movement algorithm of our numerical method and because it seems likely that similar techniques could provide a local existence result for our problem.

Consider the modified Stefan problem with an isotropic velocity-independent Gibbs–Thomson relation with $\varepsilon_C = 1$, with the heat equation replaced by its steady state counterpart $\Delta u = 0$, and with temperature variation in the solid phase neglected. The problem can then be stated in one sentence: *A curve moves with velocity equal to the normal derivative of the harmonic function with boundary values equal to the curvature of the curve.*

Thus we seek a curve $\Gamma(t)$ moving with normal velocity

$$V = \frac{\partial U}{\partial \nu},$$

where $\Delta U = 0$ above $\Gamma(t)$ and

$$U = C \qquad \text{on} \quad \Gamma(t).$$

Here C is the curvature and ν the normal of $\Gamma(t)$. Consider the special situation in which $\Gamma(t)$ is the graph $\{x = x,\ y = y(x) \mid -\infty < x < \infty\}$ of a Lipschitz function y. Parametrize $\Gamma(t)$ by arclength and let ϕ be the angle between ν and the y-axis. Let $\Lambda = \Lambda_\Gamma$ denote the Dirichlet–Neumann operator for $\Gamma = \Gamma(t)$, defined for $f \in L^2(\Gamma)$ by

$$\Lambda f = \partial U / \partial \nu,$$

where

$$\Delta U = 0 \qquad \text{above} \quad \Gamma$$
$$U = f \qquad \text{on} \quad \Gamma;$$

thus the normal velocity is given as a functional of curvature by $V = \Lambda C = \Lambda\, D\phi$. One can then derive the following evolution equation for ϕ (see [14] or Section 4 for details);

$$\partial_t \phi - D\Lambda C = C \int_0^s C\, \Lambda C\, ds', \qquad C = D\phi, \tag{1}$$

with initial condition $\phi(0, s) = \phi_0(s)$. This is a nonlinear third-order pseudodifferential evolution equation, since Λ is a first-order pseudodifferential operator [53] acting on the usual Sobolev space $H^2 = H^2(\Gamma)$ consisting of square integrable functions on Γ with square integrable first and second distributional derivatives. Let $|\phi|_\infty = \max_\Gamma |\phi|$. Then the following result holds:

THEOREM (Duchon and Robert [14]). *Let ϕ_0 belong to H^2, and $|\phi_0|_\infty < \pi/2$. (Thus $\Gamma(0)$ is a Lipschitz graph.) Then there is $T > 0$ and ϕ continuous from the interval $[0, T]$ into H^2 satisfying (1) and having $\phi(0, s) = \phi_0(s)$. Furthermore, there is a ball in $L^\infty(0, T; H^2)$ in which the solution of (1) is unique.*

Extension of this theorem to our supercooled Stefan problem would require two steps. The first—inclusion of temperature variation in the solid phase—seems to present no additional difficulties, but the second—solution of the heat equation on a time-dependent domain—is much more difficult than the solution of the Laplace equation, which does not involve the previous history of the interface. Even the solution of the equation corresponding to (1) for ϕ in terms of the right-hand side becomes a nontrivial undertaking, because Λ acts on the time variable.

However, this general viewpoint—in which the temperature field is treated as an intermediate step between the curvature and the normal velocity, rather than as an independent unknown—pervades the work of this paper. Our numerical methods are based on equations which involve only the moving boundary.

1.3. *Numerical Methods*

We briefly describe some of the many existing numerical methods for the curvature-independent classical Stefan problem without supercooling, to provide a background for our work on the curvature-dependent and supercooled case. A good general reference is the conference proceedings [58], particularly [18, 12, 41]; these articles also describe many methods which we have omitted.

Methods for the classical Stefan problem in more than one space dimension (the one-dimensional case is of little interest to us here) tend to fall into two general classes; front-tracking methods which follow the boundary explicitly and enthalpy methods which use a single-domain formulation. A general review of numerical methods for moving interfaces can be found in Hyman [30].

In front-tracking methods, the usual procedure is to solve the heat equation in each phase with zero Dirichlet data on $\Gamma(t)$ by finite element or finite difference methods, compute an approximate normal velocity from the temperature field and an approximate normal by some method depending on the representation of the moving boundary, and move the boundary with the computed velocity. Variations on this procedure include solving with Neumann data and adjusting the boundary to be where $u = 0$, or using an implicit time discretization and iterating on the temperature and the boundary until the boundary location and velocity agree with those obtained from the temperature field. Front-tracking methods have been

applied to the classical Stefan problem by Meyer [41] and to several similar problems (e.g., Rayleigh–Taylor instability) by Glimm *et al.* [25].

In enthalpy methods, the Stefan problem is transformed to a single nonlinear heat equation of the form $\partial_t u = \Delta f(u)$, with f a step function, to hold weakly on the entire domain occupied by the two phases. After computing u, the boundary may be found, if desired, as the set $\{u = 0\}$. Various methods have been proposed to solve $\partial_t u = \Delta f(u)$; Chorin [10] reports numerical experiments with the simplest finite difference method. Berger *et al.* [4] derive similar finite difference methods in a very general framework; their methods are very simple to use but have rather large temperature field error estimates of the form $O((\Delta t \log(1 + T/\Delta t))^{1/2})$, where Δt is the timestep and T is the time at which the error is bounded. Their numerical results show these estimates to be sharp. Alexander *et al.* [1] have applied moving finite elements to the enthalpy formulation. Other weak solution methods are presented in [55], with similar error estimates.

Numerical methods for the curvature-dependent supercooled Stefan problem, however, are much more scarce. Smith [48] and Chorin [10] have constructed methods based on the enthalpy formulation, but incorporating some type of front tracking to evaluate the curvature. Smith's method suffered from *grid effects*; the shape of the computed interface is strongly and unphysically dependent on the orientation of the numerical grid used to solve the problem. Smith's numerical results are thus not even qualitatively accurate in the presence of morphological instability and, in particular, do not agree with linear stability theory. Chorin [10] introduced a partial volume representation [30] of the interface and an accurate curvature evaluation algorithm for curves given by partial volumes, but this did not remove the grid effects. In addition, both of these approaches are based on the enthalpy formulation and therefore are limited to $O((\Delta t \log(1 + T/\Delta t))^{1/2})$ accuracy. Chorin's numerical results indicate that this estimate is sharp. Recently, Sullivan *et al.* [52] have solved the problem using finite element methods on a moving mesh, but their results so far are limited to the case when the interface is the graph of a function and therefore cannot follow the interface into the nonlinear regime. The convergence rate of their method is unknown, and it is not clear whether they obtain quantitative agreement with linear stability theory. In view of the incorrectness of the theory (see Section 1.5 or [49, 50]) such agreement would hardly be valuable.

Thus it seems fair to say that there are no completely satisfactory methods for solving the supercooled Stefan problem with a general anisotropic curvature- and velocity-dependent boundary condition. This paper presents a first-order accurate method which can follow the interface far into the nonlinear regime. Our method is based on solving a boundary integral equation [39, 40], and thus eliminates grid effects by eliminating the spatial grid; indeed, we eliminate the temperature field altogether. We must then solve a singular integral equation for the velocity of the moving boundary, but it turns out than this can be done quite accurately, with some attention to numerical details. Given the velocity, it is still not altogether trivial to move the curve, because the velocity is curvature-dependent. Sethian [47]

has exhibited some of the difficulties in moving curves with curvature-dependent velocity. We use a new algorithm involving an evolution equation for the normal angle, an ordinary differential equation for the arclength, and an algorithm which keeps points on the curve equidistant in arclength, to avoid the instability observed by Sethian.

1.4. *Classical Linear Stability Theory*

In this section, we review the results of the classical linear stability theory [42] of the isotropic velocity-independent Gibbs–Thomson relation

$$u = -\varepsilon C,$$

following [50]. Another approach to this analysis is presented in [44]. The predictions of this analysis will be compared with numerical results in Section 3.

Consider the planar interface in $\mathbb{R}^2$ parametrized by

$$\Gamma(t)\colon (=Vt, x=s), \qquad s\in\mathbb{R} \tag{1}$$

with temperature field

$$u(x, y, t)=\begin{cases} e^{-V(y-Vt)}-1, & y>Vt \\ 0, & y<Vt, \end{cases} \tag{2}$$

independent of x. The interface moves into the liquid phase with positive velocity V, and the temperature field propagates without change of structure.

Perturb this solution by adding temperature fields δu_S and δu_L in the solid and liquid phases, respectively, and let $y=Vt+\delta y(t, x)+O(\delta^2)$ be the resulting perturbed interface. Linearize the moving boundary problem by extending u_L and u_S up to the unperturbed boundary as solutions of the heat equation, and using Taylor expansion to construct an effective boundary condition there. The classical theory should analyze the stability of exponential solutions of the form

$$\begin{aligned} u_S &= u_0 e^{ikx} e^{y_1 t} e^{q(y-Vt)} \\ u_L &= u_0' e^{ikx} e^{y_1 t} e^{-q'(y-Vt)} \\ y(t, x) &= y_0 e^{ikx} e^{y_1 t}, \end{aligned} \tag{3}$$

by computing the linear stability exponent y_1 for all positive q and q' and real k. Unfortunately, the dispersion relations fix q and q' in terms of k (see [49, 50, 36]). But to represent an arbitrary perturbation of the initial temperature field and interface requires *three* independent parameters, q, q', and k. Thus we have too few degrees of freedom to carry out a complete stability analysis. Since the solution is stable if no modes grow, but unstable if any modes grow, we can reliably predict instability by this analysis, but not stability.

At any rate, for $\varepsilon = 0$, the classical dispersion relations imply

$$y_1 = \begin{cases} \pm V|k|, & |k| < V \\ V|k|, & |k| > V. \end{cases} \tag{4}$$

Thus the classical theory predicts instability of all modes, for $\varepsilon = 0$.

For $\varepsilon > 0$, on the other hand, one finds

$$y_1 = q(q+V) - k^2 \tag{5}$$

$$= 2\varepsilon k^2(\varepsilon k^2 - V) + (V - 2\varepsilon k^2)|k|\sqrt{1 - V\varepsilon + \varepsilon^2 k^2}. \tag{6}$$

Asymptotically,

$$y_1 \sim \begin{cases} \sqrt{1 - V\varepsilon}\, V|k|, & \text{as } k \to 0 \\ -k^2, & \text{as } k \to \infty. \end{cases} \tag{7}$$

Thus the classical theory predicts the stabilization of short waves by curvature-dependence. Unfortunately, this prediction applies only to certain specially constrained perturbations, in which q and q' are determined by k (see [49, 50, 36]).

1.5. *The Integral Equation Formulation*

In this section, we state the moving boundary problem and use heat potential theory to convert it to a singular integral equation for the interface alone. Then we summarize the results of the correct linear stability theory, following [49].

We are working with the following moving boundary problem:

$$\begin{aligned} \partial_t u &= \Delta u && \text{on } \Omega(t) \\ \partial_t u &= \Delta u && \text{on } \tilde{\Omega}(t) \\ [\partial u/\partial v] &= -V && \text{on } \Gamma(t) \\ u &= -\varepsilon_C(\phi)C - \varepsilon_V(\phi)V && \text{on } \Gamma(t) \\ u &\to u_\infty && \text{at } \infty \text{ in each phase} \\ u &= u_0 && \text{at } t = 0. \end{aligned} \tag{1}$$

The notation is as follows:

Δ	is the Laplacian $\partial_x^2 + \partial_y^2$,
$\Omega(t)$	is the solid phase at time t,
$\tilde{\Omega}(t)$	is its complement, the liquid phase,
u_∞	is the temperature at ∞ in each phase,
$v = (\cos\phi, \sin\phi)$	is the outward unit normal to $\Omega(t)$,
[ ]	denotes the difference between liquid and solid phase values,

$\Gamma(t)$	is the boundary bewteen $\Omega(t)$ and $\tilde{\Omega}(t)$,
V	is its normal velocity, positive if liquid is freezing,
C	is its curvature, positive where the solid is convex, and
ϕ	is the angle between ν and the y-axis.

In the Gibbs–Thomson relation, we take anisotropic material parameters

$$\varepsilon_C(\phi) = \varepsilon_C(1 - A\cos k_A\phi)$$
$$\varepsilon_V(\phi) = \varepsilon_V(1 - A\cos k_A\phi),$$

where ε_C and ε_V are positive constants much less than unity, A is a constant between 0 and 1, and k_A is a small integer describing the crystalline anisotropy of the substance under consideration.

In this section, we transform the moving boundary problem (1) to a singular integral equation (2) involving only $\Gamma(t)$ and the initial temperature field u_0. Supercooling is present in (2) only through the consistency requirement that $u_0 \to u_\infty$ at infinity. The procedure is straightforward. We use the free-space heat kernel

$$K(\mathbf{x}, t) = \frac{e^{-\|\mathbf{x}\|^2/4t}}{(4\pi t)^{n/2}} \qquad \mathbf{x} \in \mathbb{R}^2,\ t > 0,$$

to express u in each phase as the sum of single, double, and initial layer heat potentials with densities $\partial u/\partial \nu$, u, and u_0, respectively. We use a jump formula for the double layer potential to evaluate each expression on $\Gamma(t)$ and add the results. This procedure produces the integral equation

$$\varepsilon_C(\phi)C + \varepsilon_V(\phi)V + U(\mathbf{x}, T) + \int_0^T \int_{\Gamma(t)} K(\mathbf{x} - \mathbf{x}', T - t)\, V(\mathbf{x}', t)\, dx'\, dt = 0 \quad (2)$$

for $\mathbf{x}$ on $\Gamma(T)$. Here U is the free solution of the heat equation with initial data u_0;

$$U(\mathbf{x}, T) = K * u_0(\mathbf{x}, T) = \int_{\mathbb{R}^2} K(\mathbf{x} - \mathbf{x}', T)\, u_0(\mathbf{x}')\, dx',$$

where $*$ denotes convolution, and dx' denotes the element of integration on $\Gamma(t)$. This equation possesses nearly every possible complication: it is nonlinear (though quasilinear), history-dependent (through the dependence of SV on the previous history of the interface), and includes derivatives as well as integration over the curve. The Gibbs–Thomson relation produces a term resembling a nonlinear heat equation (for a parametrization of $\Gamma(t)$), while the release of latent heat generates the singular integro-differential term SV, which is nonlinear and history-dependent as well. The initial temperature field term U is merely a nonlinear forcing term, which adds little complexity by comparison.

The derivation goes like this: Let $T>0$ be fixed, and let $\mathbf{x}$ lie in $\Omega(T)$. Fix $\delta>0$ and put

$$f(\mathbf{x}', t) = K(\mathbf{x}-\mathbf{x}', T-t+\delta).$$

Let Ω_T be the product set

$$\Omega_T = \prod_0^T \Omega(t).$$

Then the Green identity [32] implies that

$$\int_{\Omega_T} u\,\Delta f - f\,\Delta u = \int_0^T \int_{\Gamma(t)} u\frac{\partial f}{\partial \nu} - f\frac{\partial u}{\partial \nu}$$

and the divergence theorem on Ω_T reads

$$\int_{\Omega_T} \partial_t(fu) = \int_{\partial\Omega_T} fun_t.$$

Here n_t is the time component of the outward unit normal to Ω_T, considered as a subset of $\mathbb{R}^2 \times \mathbb{R}^+$;

$$n_t = \begin{cases} 1 & t=T,\ \mathbf{x}\in\Omega(T) \\ -1 & t=0,\ \mathbf{x}\in\Omega(0) \\ \dfrac{-V}{\sqrt{1+V^2}} & 0<t<T,\ \mathbf{x}\in\Gamma(t). \end{cases}$$

Add these two formulas, use the backward heat equation satisfied by f, and take the limit $\delta\to 0$ to get

$$u(\mathbf{x}, T) = \int_{\Omega(0)} fu_0 - \int_0^T \int_{\Gamma(t)} fun_t - f\frac{\partial u}{\partial \nu} + u\frac{\partial f}{\partial \nu} \tag{3}$$

for $\mathbf{x}$ in $\Omega(T)$. Repeat the calculation for the liquid phase; only the sign of the double integral changes;

$$u(\mathbf{x}, T) = \int_{\tilde{\Omega}(0)} fu_0 + \int_0^T \int_{\Gamma(t)} fun_t - f\frac{\partial u}{\partial \nu} + u\frac{\partial f}{\partial \nu} \tag{4}$$

for $\mathbf{x}$ in $\tilde{\Omega}(T)$. Now we need a jump formula for the double layer heat potential D defined by

$$Dg(\mathbf{x}, T) = \int_0^T \int_{\Gamma(t)} g(\mathbf{x}', t)\frac{\partial K}{\partial \nu}(\mathbf{x}-\mathbf{x}', T-t)\,dx'\,dt;$$

Dg is discontinuous across $\Gamma(T)$. For $\Gamma(t)$ smooth, it is shown formally in [50] that

$$[Dg](\mathbf{x}, T) = g(\mathbf{x}, T) \tag{5}$$

for $\mathbf{x}$ on $\Gamma(T)$. A proof of (5) for $\Gamma(T)$ independent of T appears in Fabes and Riviere [17]; they use a Fourier transform in the time variable to reduce it to potential theory for the Laplace equation [21] in which the jump condition is well known. This case is easier than ours because there is no motion of the boundary: the Fourier transform approach fails at the first step when the boundary moves with time. A proof for $\Gamma(T)$ time-dependent can be found in [24] for $n=1$. Apparently no proof of the jump formula with $\Gamma(t)$ time-dependent has been published for $n>1$, so we will rely on the formal argument presented in [50].

Thus apply the jump formula to evaluate the expressions (3) and (4) for u on $\Gamma(t)$ and add the results to get

$$u(\mathbf{x}, T) = \int_{\mathbb{R}^2} K(\mathbf{x}-\mathbf{x}', T-t)\, u_0(\mathbf{x}') - \int_0^T \int_{\Gamma(t)} K(\mathbf{x}-\mathbf{x}', T-t) \left[\frac{\partial u}{\partial \nu}\right] dx'\, dt$$

for $\mathbf{x}$ on $\Gamma(T)$. The boundary conditions now imply (2):

$$\varepsilon_C(\phi) C + \varepsilon_V(\phi) V + U(\mathbf{x}, T) + \int_0^T \int_{\Gamma(t)} K(\mathbf{x}-\mathbf{x}', T-t)\, V(\mathbf{x}', t)\, dx'\, dt = 0, \tag{6}$$

for $\mathbf{x}$ on $\Gamma(T)$.

Remarks. 1. Although K has a $1/(T-t)$ singularity at $t=T$, the actual singularity of the integrand in the time integral is mollified to a square root by integration over the curve. To see this, we compute the asymptotic behavior of the curve integral as $t \to T$. Parametrize $\Gamma(t)$ by $\mathbf{x}(t, s)$, and let $\mathbf{x} = \mathbf{x}(S, T) \in \Gamma(T)$. Then $dx' = \sqrt{x_s^2 + y_s^2}\, ds$ and

$$\int_{\Gamma(t)} K(\mathbf{x}-\mathbf{x}', T-t)\, V(\mathbf{x}', t)\, dx' = \int_{-\infty}^{\infty} K(\mathbf{x}-\mathbf{x}', T-t)\, V(s, t) \sqrt{x_s^2 + y_s^2}\, ds.$$

It is easy to see that only a neighborhood of the singularity contributes, because K decays exponentially in the spatial variables. But in a small enough neighborhood of the singularity, the Taylor expansion

$$\|\mathbf{x}(S, T) - \mathbf{x}(s, t)\|^2 = (S-s)^2 (x_s^2 + y_s^2) + \|\mathbf{x}(S, T) - \mathbf{x}(S, t)\|^2 + \cdots$$

holds with a negligible error. The second term, exponentiated, gives a s-independent factor in the integrand with the first term a Gaussian integral. The result is therefore

$$\int_{\Gamma(t)} K(\mathbf{x}-\mathbf{x}', T-t)\, V(\mathbf{x}', t)\, dx'$$
$$\sim K(\|\mathbf{x}(S, T)-\mathbf{x}(S, t)\|, T-t)\, V(S, t) \qquad \text{as} \quad t' \to t, \tag{7}$$

where on the right-hand side K denotes the one-space-dimensional heat kernel.

2. To simplify the notation, introduce the single layer potential operator S defined by

$$SV(\mathbf{x}, T) = \int_0^T \int_{\Gamma(t)} K(\mathbf{x}-\mathbf{x}', T-t)\, V(\mathbf{x}', t)\, dx'\, dt \tag{8}$$

and write the integral equation as

$$\varepsilon_C C + U(\mathbf{x}, T) + (\varepsilon_V + S) V = 0. \tag{9}$$

As an integral equation for V, this is of the second kind when $\varepsilon_V \neq 0$. Since first-kind equations with compact smoothing operators (as S is) are notoriously hard to solve, we expect velocity-dependence to make the solution of the integral equation easier. Taking $\varepsilon_V \neq 0$ can thus be thought of as a physically motivated *regularization* of the $\varepsilon_V = 0$ problem. The velocity is therefore given in terms of $\Gamma(t)$ by

$$V = -(\varepsilon_V + S)^{-1} (\varepsilon_C C + U),$$

if $\varepsilon_V + S$ is invertible in an appropriate function space. Fabes and Riviere [17] show, for $\Gamma(t)$ independent of t, that S is smoothing of order 1 in space and order $\frac{1}{2}$ in time: If g is in L^p on the set

$$\Gamma_T = \prod_0^T \Gamma(t),$$

then Sg has one space derivative in $L^p(\Gamma_T)$ and—in a sense we shall not make precise—half a time derivative in $L^p(\Gamma_T)$. They also show that $\varepsilon_V + S$ is invertible on $L^p(\Gamma_T)$ if and only if $\varepsilon_V \neq 0$. If ε_V vanishes, therefore, V loses one derivative's worth of spatial regularity. Hence nontrivial velocity-dependence in the Gibbs–Thomson relation exerts a substantial smoothing effect on the interfacial velocity.

Now we describe the correct stability theory, based on the integral equation formulation. The integral equation (1.5.6) has an exact solution for which the interface is a straight line given by (1.4.1) and the temperature field has the similarity form

$$u(x, y, t) = u_0(y - Vt) \tag{10}$$

with

$$u_0(y) = \begin{cases} e^{-Vy} - 1 - \varepsilon_V V, & y > 0 \\ -\varepsilon_V V, & y \leqslant 0. \end{cases} \tag{11}$$

Here ε_V is evaluated at its minimum, $\phi = 0$.

We compute the evolution of a small perturbation to the initial interface, subject to a small perturbation of the initial temperature field, within the framework of linear stability theory. Make a perturbation $\delta u_1(x, y)$ of the initial temperature field $u_0(y)$, and let the resulting interface be parametrized by

$$x(t, s) = s + O(\delta^2)$$
$$y(t, s) = Vt + \delta y_1(t, s) + O(\delta^2).$$

A calculation as in [50] results in a linear stability equation

$$(2\varepsilon_V \partial_t + 2\varepsilon_C k^2 - V)\, g(t) + \int_0^t \frac{e^{-(k^2 + V^2/4)(t-s)}}{\sqrt{\pi(t-s)}} \left(\partial_s + \frac{V^2}{2}\right) g(s)\, ds$$
$$= e^{-(k^2 + V^2/4)t}\, F(t), \tag{12}$$

where

$$F(t) = -2e^{V^2 t/4} K * f(Vt, t) \tag{13}$$

and we are studying the evolution of a single harmonic

$$y_1(t, s) = g(t) e^{iks}.$$

The change of unknown function

$$G(t) = e^{(k^2 + V^2/4)t}\, g(t) \tag{14}$$

produces a fractional differential equation

$$[cD + b + D^{-1/2}(D - a)]\, G(t) = F(t), \tag{15}$$

with constant coefficients

$$a = k^2 - V^2/4, \qquad b = 2\varepsilon_C k^2 - V - 2\varepsilon_V k^2 - \varepsilon_V \frac{V^2}{2}, \qquad c = 2\varepsilon_V. \tag{16}$$

Here $D = \partial_t$ and $D^{-1/2}$ is the Riemann–Liouville fractional integral [38] defined by

$$D^{-1/2} G(t) = \int_0^t \frac{g(s)}{\sqrt{\pi(t-s)}}\, ds. \tag{17}$$

The fractional differential equation (15) can be solved explicitly if we take f of the form

$$f(y) = \begin{cases} u_0' e^{-q'y}, & y > 0 \\ u_0 e^{-qy}, & y < 0 \end{cases} \tag{18}$$

with q and q' positive. By a Laplace transform, this implies the solution for the general case. F then becomes

$$F(t) = -u_0' \operatorname{erfce}(p' \sqrt{t}) - u_0 \operatorname{erfce}(p \sqrt{t}) \tag{19}$$

with $p = q + V/2$, $p' = q' - V/2$. If $G(p, t)$ is the solution corresponding to $u_0 = -1$, $u_0' = 0$, then G is given by

$$G(t) = -u_0 G(p, t) - u_0' G(p', t).$$

Thus it suffices to consider

$$F(t) = \operatorname{erfce}(p \sqrt{t}) = (1 - pD^{-1/2}) e^{p^2 t}. \tag{20}$$

The second equality, derived by a change of variable, greatly simplifies the calculation.

The solution of (15) is as follows: We solve the $c = 0$ (no velocity dependence) case explicitly by "squaring" the operator in (15) to remove fractional derivatives (see [50]). The result is an ordinary differential equation for the time-dependent amplitude g, whose solution is asymptotically a linear combination of exponentials

$$g(t) \sim \sum_{i=1}^{2} g_i(k) e^{t y_i}, \qquad \text{as} \quad t \to \infty.$$

Thus, in the long-time limit, stability theory is reduced to the study of the exponents y_i and amplitudes $g_i(k)$. It turns out that y_1 is briefly positive for small k and then decays like $-k^2$ for large k. Unfortunately, $y_2 \sim k^4$ as $k \to \infty$, so it looks at first as though the interface is catstrophically unstable. However, a slight additional calculation reveals that $g_2(k)$ vanishes identically for k above a cutoff k_c. Thus the high-k instability is indeed stabilized by the introduction of curvature dependence in the Gibbs–Thomson relation, just as predicted by the classical theory. The same picture appears in the case $c > 0$ of nontrivial velocity dependence, except that y_i are now roots of a cubic rather than a quadratic. See [51 or 49] for details. The algebra involved in exhibiting the cutoff directly becomes too formidable, but a calculation presented in [49] effectively bounds the cutoff from above. This calculation exhibits the stabilizing effect of velocity-dependence: the cutoff k_c is lowered even further. The effects of anisotropy, on the other hand, are much easier to include in the analysis.

It turns out that any instability is cut off by the vanishing of its coefficient whenever k exceeds a cutoff k_c bounded by

$$k_c^2 \leqslant \frac{V}{2(1-A)\varepsilon_C}. \tag{21}$$

Thus, to summarize, linear stability analysis of the (approximately generic) planar constant-speed solution shows that the curvature-dependent Gibbs–Thomson relation replaces the catastrophic small-scale instability of the classical Stefan problem for supercooled water by a finite band of small-k unstable modes. Velocity dependence further narrows this band. Anisotropy tends to destabilize the situation, replacing ε_C and ε_V by $(1-A)\varepsilon_C$ and $(1-A)\varepsilon_V$.

Note also that the integral equation approach gives results which agree with the classical theory *only* in the long-time limit. The relevance of this limit is not clear *a priori*, because linear stability theory is a small-amplitude paradigm and both calculations indicate that some modes are almost always growing. Thus the theory may well break down long before the long-time limit is approached; if this happens, the classical theory would be invalidated, but the new theory would not.

2. Numerical Methods for Periodic Graphs

2.1. *Introduction*

This section contains a numerical method for computing the moving boundary $\Gamma(t)$ when it is representable as the graph $\{x=s,\ y=y(t,s) \mid -\infty < s < \infty\}$ of a 2π-periodic function $y(t,x)$ of x. Thus we compute an infinite periodic array of dendritic structures. After specializing the integral equation formulation to such a periodic graph, we discretize the curve, replacing it by a set of points. This produces a consistency condition on the time and space step sizes Δt and Δs. Then we present a heuristic analysis which exhibits the importance of the high-wavenumber behavior of the curvature approximation. The interface can be destabilized by a local curvature discretization if Δs is too large; we use the discrete Fourier transform to construct a discretization of curvature which avoids this difficulty.

the interface is flat. After using the understanding gained from the planar case to discretize the full periodic equation of motion, we present numerical results which demonstrate first-order accuracy of the method and agree with the linear stability theory presented in Section 1.5. Our results disagree with the classical linear stability theory.

Working first with periodic graphs allows us to learn how to compute the velocity without worrying about the complications of moving a general curve; general curves are considered in Section 3. In general, we study each part of our method in a simple situation where analysis is easy.

2.2. *The Periodic Graph Equation of Motion*

In Section 1.5, we derived the integral equation

$$\varepsilon_C(\phi) C + \varepsilon_V(\phi) V + U(\mathbf{x}, t) + \int_0^t \int_{\Gamma(t')} K(\mathbf{x} - \mathbf{x}', t - t')\, V(\mathbf{x}', t')\, dx'\, dt' = 0 \tag{1}$$

for a parametrization $\mathbf{x} = \mathbf{x}(t, s)$ of $\Gamma(t)$. Primes denote evaluation at primed variables, and dx' is the element of integration on $\Gamma(t')$. While $\Gamma(t)$ remains a periodic graph, we can work with the special parametrization

$$x = s$$

$$y = y(t, s),$$

where y is 2π-periodic in s. Then the curvature, normal velocity, and element of arclength are given by [9, 57]

$$C = -\partial_s \frac{y_s}{\sqrt{1 + y_s^2}}, \tag{2}$$

$$V = \frac{\partial_t y}{\sqrt{1 + y_s^2}}, \tag{3}$$

$$dx' = \sqrt{1 + y_s^2}\, ds'.$$

Periodicity makes the problem simpler by restricting the variable s to a finite interval. Indeed, if y is 2π-periodic then

$$\begin{aligned} &\int_{-\infty}^{\infty} K(s - s', y - y', t - t')\, \partial_t y'\, ds' \\ &= \sum_{-\infty}^{\infty} \int_{-\pi}^{\pi} K(s - (2n\pi + s'), y - y', t - t')\, \partial_t y'\, ds' \\ &= \int_{-\pi}^{\pi} \Theta(s - s', t - t')\, K(y - y', t - t')\, \partial_t y'\, ds', \end{aligned}$$

where Θ is the Jacobi theta function [16] or periodic heat kernel [32] defined by

$$\Theta(s, t) = \sum_{-\infty}^{\infty} K(s + 2n\pi, t) \tag{4}$$

and K is now the one-dimensional Gauss kernel. Thus the integral equation becomes

$$\varepsilon_C(\phi) C + \varepsilon_V(\phi) V + U(\mathbf{x}, t) + \int_0^t \int_{-\pi}^{\pi} \Theta(s - s', t - t')\, K(y - y', t - t')\, \partial_t y'\, ds'\, dt' = 0, \tag{5}$$

to hold for $-\pi \leqslant s \leqslant \pi$, with periodic boundary conditions.

The elementary properties of the theta function which we shall need all flow from the Poisson summation formula [16]. As an example, we derive an efficient algorithm for evaluating Θ numerically. The sum (4) converges very fast for small t, since then

$$K(x, t) = \frac{e^{-x^2/4t}}{\sqrt{4\pi t}} \tag{6}$$

decays very fast as $x \to \infty$. For t large, however, convergence is extremely slow. Thus we use the Poisson summation formula

$$\sum_{-\infty}^{\infty} f(k) = \sum_{-\infty}^{\infty} \hat{f}(k)$$

to transform the sum (4) defining Θ. Here $\hat{f}$ denotes the Fourier transform

$$\hat{f}(k) = \int_{-\infty}^{\infty} e^{2\pi i k x} f(x)\, dx,$$

so that for each fixed t, evaluation of a Gaussian integral gives

$$\hat{K}(k, t) = \frac{1}{2\pi} e^{-tk^2}.$$

Hence Θ is also given by

$$\Theta(s, t) = \frac{1}{2\pi} \sum_{-\infty}^{\infty} e^{iks} e^{-k^2 t}, \tag{7}$$

which is its Fourier series representation. The error in truncating the series (7) after terms with $|k| = N - 1$ can be bounded by a geometric series; we have

$$\left| \frac{1}{2\pi} \sum_{|k| \geqslant N} e^{-k^2 t} e^{iks} \right| \leqslant \frac{1}{\pi} \sum_{N}^{\infty} e^{-Nkt} = \frac{1}{\pi} \frac{e^{-N^2 t}}{1 - e^{-Nt}}.$$

Similarly, for $|s| \leqslant 2\pi$ and $|n| \geqslant N + 1$, we have $(s + 2n\pi)^2 \geqslant 4\pi^2 N(|n| - 1)$. Hence the error in truncating (4) after terms with $|n| = N$ is bounded by

$$\begin{aligned} \frac{1}{\sqrt{4\pi t}} \sum_{|n| \geqslant N+1} e^{-(s+2n\pi)^2/4t} &\leqslant \frac{1}{\sqrt{\pi t}} \sum_{n=N+1}^{\infty} e^{-\pi^2 N(n-1)/t} \\ &= \frac{1}{\sqrt{\pi t}} \frac{e^{-\pi^2 N^2/t}}{1 - e^{-\pi^2 N/t}}. \end{aligned}$$

The two error bounds are equal when $t = \pi$, which suggests the following

ALGORITHM.

if $t \leqslant \pi$ **then**

$$\Theta(s,t) \cong \frac{1}{\sqrt{4\pi t}} \sum_{-N}^{N} e^{-(s-2\pi k)^2/4t}$$

else if $t > \pi$ **then**

$$\Theta(s,t) \cong \frac{1}{2\pi}\left(1 + 2\sum_{1}^{N} \cos(ks) e^{-k^2 t}\right). \tag{8}$$

Its absolute error is bounded by

$$\frac{1}{\sqrt{\pi}} \frac{e^{-\pi N^2}}{1-e^{-\pi N}} \frac{1}{\sqrt{\min(t,\pi)}},$$

which is less that $3 \cdot 10^{-11}$ for $t > 10^{-4}$ and $N = 3$. Thus Θ can be evaluated at the cost of half a dozen exponentials, with enough accuracy for our purposes. This is important, because the major cost of our numerical method will be evaluation of the single layer potential, which requires many evaluations of Θ.

2.3. *Curve Discretization*

In this section, we discretize the periodic integral equation (2.2.5) in the spatial variable s to produce a semidiscrete equation of motion. Let $s_j = j\,\Delta s = j\pi/J$ with $-J \leqslant j \leqslant J$, and let $y_j(t)$ approximate $y(t, s_j)$. Replace C and V by

$$C_j = -D\frac{Dy_j}{\sqrt{1+Dy_j^2}} \tag{1}$$

$$V_j = \frac{\partial_t y_j}{\sqrt{1+Dy_j^2}}, \tag{2}$$

where D is a discrete approximation of ∂_s, left unspecified for moment.

Next, replace the s'-integral by a numerical integration rule. Because of periodicity, the trapezoidal rule is attractive. But $\Theta(s,t)$ becomes a point mass $\delta(s)$ as $t \to 0$, so we cannot use a trapezoidal sum all the way up to $t' = t$. Hence we study the error in the trapezoidal rule approximation to the convolution $\Theta * g$;

$$\frac{\pi}{J}\sum_{-J}^{J}{}' \Theta(s-s_j, t)\, g(s_j) \cong \Theta * g(s,t) = \int_{-\pi}^{\pi} \Theta(s-s', t)\, g(s')\, ds'. \tag{3}$$

Here J is a positive integer, $s_j = j\,\Delta s = j\pi/J$, and the prime on the sum means that the first and last terms of the sum are halved.

By a Fourier series expansion, it is enough to analyze the error for exponentials $g(s) = e^{iks}$ with integer wavenumber k. Then by the geometric series formula

$$\frac{\pi}{J}\sum_{-J}^{J}{}' e^{iks_j} = \begin{cases} 2\pi, & k \equiv 0 \pmod{2J} \\ 0, & \text{otherwise,} \end{cases}$$

the trapezoidal approximation (3) becomes

$$\frac{\pi}{J}\sum_{-J}^{J}{}' \Theta(s-s_j,\, t)e^{iks_j} = \frac{1}{2\pi}\sum_{-\infty}^{\infty} e^{-n^2t}e^{ins}\frac{\pi}{J}\sum_{-J}^{J}{}' e^{i(k-n)s_j} \tag{4}$$

$$= e^{iks}\left(e^{-k^2t} + \sum_{n\neq 0} e^{-(k+2Jn)^2t}e^{2Jins}\right). \tag{5}$$

(Incidentally, it follows that exponentials are eigenfunctions of the discrete Θ-kernel, since the parenthesized term on the right of (5) is independent of j when s is restricted to the set $\{s_j \mid -J \leqslant j < J\}$. This will be useful in the next section.) Rearranging the exponents shows that (5) is equal to

$$e^{-k^2t}e^{iks}2\pi\Theta(2J(s+ikt),\, 4J^2t) = \Theta * g(s,\, t) + O(e^{-4J^2t}) \qquad \text{as} \quad J^2t \to \infty, \tag{6}$$

$$= O(1/\sqrt{J^2t}) \qquad \text{as} \quad J^2t \to 0, \tag{7}$$

Thus the trapezoidal sum approximates $\Theta * g$ with an error which decays exponentially as $J^2t \to \infty$, but blows up like $1/\sqrt{J^2t}$ as $J^2t \to 0$. Hence we can use the trapezoidal rule up to a time cutoff Δt away from $t' = t$, if we arrange to have $J^2\,\Delta t \to \infty$ as the mesh size and cutoff are refined.

Now we return to our real interest, the integral

$$\int_{-\pi}^{\pi} K(y-y',\, t-t')\,\Theta(s-s',\, t-t')\,\partial_t y(s',\, t')\,ds'. \tag{8}$$

The previous analysis suggests the following procedure: Approximate (8) by the trapezoidal rule for $t' < t - \Delta t$, for some cutoff Δt. For $t' \geqslant t - \Delta t$, replace (8) by its asymptotic value (1.5.7);

$$\int_{-\pi}^{\pi} K(y-y',\, t-t')\,\Theta(s-s',\, t-t')\,\partial_t y(s',\, t')\,ds'$$

$$\sim K(y(t,\, s)-y(t',\, s),\, t-t')\,\partial_t y(t',\, s)$$

as $t' \to t$.

Finally, substitute the discrete curvature and velocity (1) and (2) and this approximation of the s'-integral (8) into the periodic graph equation of motion (2.2.5) to get the semidiscrete equation of motion

$$\varepsilon_C C_j + \varepsilon_V V_j + U(s_j,\, y_j,\, t)$$

$$+ \int_0^{t-\Delta t} \Delta s \sum_{-J}^{J}{}' \Theta(s_j - s_k,\, t-t')\,K(y_j - y_k',\, t-t')\,\partial_t y_k'\,dt'$$

$$+ \int_{t-\Delta t}^{t} K(y_j - y_j',\, t-t')\,\partial_t y_j'\,dt' = 0. \tag{9}$$

Consistency requires that $J^2\,\Delta t \to \infty$ as $J \to \infty$, $\Delta t \to 0$. We usually satisfy this condition by setting $J\,\Delta t = 1$.

2.4. *Curvature Distretization and Linear Stability*

In this section, we analyze the effect of curvature discretization on the linear stability of the interface, and thereby construct an appropriate curvature approximation. Let $\varepsilon_V = 0$ for ease of calculation, so the semidiscrete equation is

$$\begin{aligned}\varepsilon_C C_j &+ U(s_j, y_j, t) \\ &+ \int_0^{t-\Delta t} \Delta s \sum_{-J}^{J}{}' \Theta(s_j - s_k, t-t')\, K(y_j - y_k', t-t')\, \partial_t y_k'\, dt' \\ &+ \int_{t-\Delta t}^{t} K(y_j - y_j', t-t')\, \partial_t y_j'\, dt' = 0. \end{aligned} \tag{1}$$

The flat interface is given by $y(t, s) = Vt$. This solution satisfies the semidiscrete equation (1) up to a residual R satisfying

$$\begin{aligned} 0 < R &= \int_0^{t-\Delta t} K(V(t-t'), t-t')\, V \left[\Delta s \sum_{-J}^{J}{}' \Theta(s_j - s_k, t-t') - 1 \right] dt' \\ &= 2V \sum_{1}^{\infty} e^{-4J^2 n^2 \Delta t} \int_0^{\infty} K(Vs, s)\, ds = O(e^{-4J^2 \Delta t}) \end{aligned} \tag{2}$$

as $J^2\, \Delta t \to \infty$. In this section, we ignore errors of exponential order in $J^2\, \Delta t$, assuming $J^2\, \Delta t$ is fairly large. Because these errors are precisely those due to numerical integration over the curve, this is equivalent to studying the exact periodic graph equation (2.2.5) with curvature C replaced by

$$C_j = -D \frac{Dy_j}{\sqrt{1 + Dy_j^2}},$$

and not discretizing the curve itself. As in Section 1.5, consider a perturbed solution

$$u_0(x, y) = u_0(y) + \delta u_1(x, y)$$

$$y_j(t) = Vt + \delta y_j(t).$$

Let L be the linearized discrete curvature operator;

$$Ly_j = \lim_{\delta \to 0} \frac{C_j(\delta) - C_j(0)}{\delta} = -D^2 y_j,$$

so that

$$C_j = \delta L y_j + O(\delta^2)$$

as $\delta \to 0$. Then the linear stability equation is

$$\begin{aligned}
&\varepsilon_C L y_j(t) + y_j(t)\, \partial_y U_0(Vt, t) + U_1(s_j, Vt, t) \\
&\quad + \int_0^{t-\Delta t} \Delta s \sum_{-J}^{J}{}' K(V(t-t'), t-t') \\
&\quad \times \left[\partial_t y_k' - \frac{V^2}{2}(y_j - y_k') \right] \Theta(s_j - s_k, t-t')\, dt' \\
&\quad + \int_{t-\Delta t}^{t} K(V(t-t'), t-t') \left[\partial_t y_j' - \frac{V^2}{2}(y_j - y_j') \right] dt' = 0,
\end{aligned}$$

where U_0 and U_1 are the zero-order and first-order temperature fields defined in [49, 51]. In the previous section, we saw that

$$\Delta s \sum_{-J}^{J}{}' e^{iks_j} \Theta(s_j - s_k, t) = e^{-k^2 t} e^{iks_j} (1 + O(e^{-4J^2 t})),$$

with the last factor independent of j. Hence we can still produce separated solutions of the form

$$\begin{aligned}
u_1(x, y) &= e^{ikx} f(y) \\
y_j(t) &= e^{iks_j} g(t).
\end{aligned}$$

The reduced equation for g is then, modulo terms of order $e^{-4J^2 t}$,

$$(2\varepsilon_C \hat{L} - V)\, g(t) + \int_0^t \frac{e^{-(k^2 + V^2/4)(t-s)}}{\sqrt{\pi(t-s)}} \left(\partial_s + \frac{V^2}{2} \right) g(s)\, ds = F(t),$$

where F is given by (1.5.13) and $\hat{L}$ is the symbol of the linearized curvature operator L;

$$\hat{L} = e^{-iks_j} L e^{iks_j},$$

where L acts on s_j. This is the same as Eq. (1.5.12) in the exact theory, except that k^2 is replaced by $\hat{L}$ in the first term. Hence we can repeat the calculation described in Section 1.5 to get a discrete exponent

$$y_1^{\sim} = 2\varepsilon_C \hat{L}(\varepsilon_C \hat{L} - V) + (V - 2\varepsilon_C \hat{L}) \sqrt{k^2 + \varepsilon_C \hat{L}(\varepsilon_C \hat{L} - V)}.$$

The exact exponent, by comparison, is given by (1.4.6), restricted to integer k by 2π-periodicity:

$$y_1 = 2\varepsilon_C k^2(\varepsilon_C k^2 - V) + (V - 2\varepsilon_C k^2) \sqrt{k^2 + \varepsilon_C k^2(\varepsilon_C k^2 - V)}.$$

Almost any reasonable curvature approximation will have $\hat{L}(k) - k^2$ and therefore $y_1^{\sim} \to y_1$, for each k, as $J \to \infty$. But finite difference approximations to C

typically represent low-k behavior of the exact symbol k^2 much better than high-k behavior. This causes trouble for $|k|$ near J. Consider, for example, the simplest finite difference approximation to the curvature; let

$$C_j = -\frac{D_+ D_- y_j}{(1 + D_+ y_j^2)^{3/2}}, \tag{3}$$

where $D_\pm$ are the usual (periodic) finite difference approximations to the derivative

$$\hat{L} = \frac{4}{\pi^2} \sin^2(\pi k / 2J).$$

As $J \to \infty$, $\hat{L} \to k^2$ for any fixed k. However, for J fixed and ε_C of any reasonable size, the numerical and exact dispersion relations can have very different behavior for $|k|$ near J; see Fig. 1a. The finite difference approximation (3) can produce a catastrophic small-scale instability, if Δs is not small enough. This can be cured by taking a finer mesh, as in Fig. 1b. Nevertheless, this phenomenon reflects a rather unpleasant sensitivity to discretization of the supercooled Stefan problem, perhaps tending to confirm the misgivings put forth in [10].

Thus it is essential to have a curvature approximation for which the linearized curvature operator has the right symbol k^2, or at least a symbol which—substituted into $\tilde{y}_1$—damps those modes which should be damped. The simplest way to do this is to take

$$C_j = -D \frac{Dy_j}{\sqrt{1 + Dy_j^2}}, \tag{4}$$

where D is designed to have symbol ik. (Equivalently, C_j is the exact curvature of a trigonometric polynomial interpolating the points (s_j, y_j).) To do this, represent y_j by the trapezoidal discrete Fourier transform pair [31]

$$y_j = \frac{1}{\sqrt{2J}} \sum_{-J}^{J}{}' e^{ijs_k} \hat{y}_k \tag{5}$$

$$\hat{y}_k = \frac{1}{\sqrt{2J}} \sum_{-J}^{J}{}' e^{-iks_j} y_j. \tag{6}$$

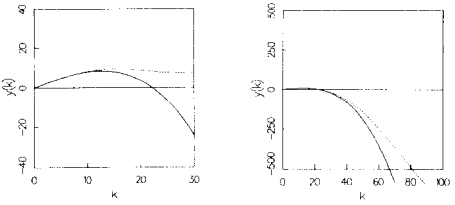

FIG. 1. Exact and discrete linear stability exponents $y_1(k)$ and $\tilde{y}_1(k)$. On the left, $\varepsilon_C = 0.001$, $J = 30$, and the numerical approximation introduces a small-case instability. On the right, $\varepsilon_C = 0.001$, but $J = 100$; this is enough points to damp the instability.

Define D^α, for $\alpha = 1$ or 2, by requiring $\widehat{D^\alpha} = (ik)^\alpha$;

$$D^\alpha y_j = \frac{1}{\sqrt{2J}} \sum_{-J}^{J}{}' (ik)^\alpha e^{ijs_k} \hat{y}_k = \sum_{-J}^{J}{}' D^\alpha_{jk} y_k,$$

so that D^α_{jk} are the trapezoidal matrix elements of D^α. Some tedious algebra involving sums of finite geometric series shows that

$$\begin{aligned}
D_{jk} &= \frac{(-1)^{j-k}}{2} \cot\left(\frac{(j-k)\pi}{2J}\right), && j \neq k \\
D_{jk} &= 0, && j = k \\
D^2_{jk} &= \frac{(-1)^{j-k+1}}{2} \csc^2\left(\frac{(j-k)\pi}{2J}\right), && j \neq k \\
D^2_{jk} &= -\frac{1}{6}(1+2J^2), && j = k.
\end{aligned} \tag{7}$$

Now this method will have the right linearized behavior, if the consistency condition

$$J^2 \Delta t \to \infty \qquad \text{as} \quad J \to \infty, \Delta t \to 0 \tag{8}$$

is satisfied. To get a reasonable approximation to a given physical situation with a practical J, we will need to capture at least all growing modes. For $V\varepsilon \ll 1$, the exponent y_1 changes sign when $k^2 \cong V/2\varepsilon_C$, so we require $J \geqslant \sqrt{V/2\varepsilon_C}$ to get a reasonable approximation. Typical test parameters [10, 52] like $V = 1$, $\varepsilon_C = 0.01$ require $J \geqslant 7$ which is not hard to satisfy. Velocity dependence weakens this requirement, but a nonzero coefficient of anisotropy A makes it more stringent by replacing ε_C with $(1-A)\varepsilon_C$. Thus in general we need roughly [see (1.5.21)]

$$J^2 \geqslant \frac{V}{2(1-A)\varepsilon_C}$$

to capture all growing modes, assuming ε_C and ε_V are much smaller than unity.

2.5. *Time Discretization*

So far we have discretized the spatial variable and found out how to get the right linearized behavior, if the consistency condition (2.4.8) is satisfied. Now we discretize the time variable. It is helpful to begin with the planar case, i.e., with the periodic graph equation specialized to $y(t, s)$ independent of s,

$$\varepsilon_V \partial_t y(t) + U(y(t), t) + \int_0^t K(y(t) - y(t'), t - t')\, \partial_t y(t')\, dt' = 0. \tag{1}$$

(Here ε_V is evaluated at $\phi = 0$.) Since curve discretization effects are not present, this allows us to study time discretization in a simpler environment than the full equation (2.3.9). A time discretization method which fails here can presumably be eliminated, though one which works here may still fail in the general case.

To produce a time discretization, replace y by a continuous piecewise linear approximation; let

$$y(t) \cong y^n + \frac{t - n\,\Delta t}{\Delta t}(y^{n+1} - y^n) = y^{n+\alpha}$$
$$\text{for} \quad n\,\Delta t < t = (n+\alpha)\,\Delta t \leqslant (n+1)\,\Delta t \tag{2}$$

and require (1) to hold at the mesh points $t = n\,\Delta t$. The resulting numerical equations are

$$\varepsilon_V \frac{y^n - y^{n-1}}{\Delta t} + U(y^n, n\,\Delta t) + \sum_{m=0}^{n-1} (y^{m+1} - y^m)$$
$$\times \int_0^1 K(y^n - y^{m+\alpha}, (n-m-\alpha)\,\Delta t)\,d\alpha = 0. \tag{3}$$

We must also choose some method of evaluating the *weights*

$$\int_0^1 K(y^n - y^{m+\alpha}, (n-m-\alpha)\,\Delta t)\,d\alpha \tag{4}$$

because only the top weight, with $m = n-1$, can be evaluated in closed form. (It is simply

$$\frac{1}{y^n - y^{n-1}} \operatorname{erf}\left(\frac{y^n - y^{n-1}}{\sqrt{4\Delta t}}\right)$$

where

$$\operatorname{erf}(z) = \frac{2}{\sqrt{\pi}} \int_0^z e^{-y^2}\,dy$$

is the error function.) We choose to evaluate them by Gaussian quadrature [13] for $m \leqslant n-2$. Satisfactory error bounds can be given for evaluating (4) by Gaussian quadrature, because the integrands in (4) with $m \leqslant n-2$ have the square-root singularity of K sufficiently distant from the interval of integration. The importance of accurate weight evaluation is well known in the theory of numerical solution of integral equations; see [28]. It is thus a stroke of good fortune that the top weight, which contains the singularity of the single layer potential, can be evaluated in closed form.

$$\varepsilon_V \frac{y^n - y^{n-1}}{\Delta t} + U(y^n, n\,\Delta t) + \operatorname{erf}\left(\frac{y^n - y^{n-1}}{\sqrt{4\Delta t}}\right) + \sum_{m=0}^{n-2} (y^{m+1} - y^m)$$
$$\times \int_0^1 K(y^n - y^{m+\alpha}, (n-m-\alpha)\,\Delta t)\,d\alpha = 0.$$

for y^n, at each time step. Newton's method is suitable for this.

We found this method to be stable and at least first-order accurate, with sufficiently accurate weight evaluation; typically 6-point Gaussian quadrature sufficed for this. Newton's method converges quickly, taking no more than five iterations to reduce the residual below 10^{-10} in double precision (14-digit) arithmetic. We carried out numerical experiments using the Neumann solution [27]. Results indicate that this time discretization method has $O(\Delta t^{3/2})$ error; since we have a first-order accurate spatial discretization, this suffices for our purposes. See [51] for details.

This time discretization method can now be applied to the periodic graph equation of motion. Let

$$y_j(t) = y_j^n + \frac{t - n\,\Delta t}{\Delta t}(y_j^{n+1} - y_j^n) = y_j^{n+\alpha}$$
$$\text{for} \quad n\,\Delta t < t = (n+\alpha)\,\Delta t \leqslant (n+1)\,\Delta t \tag{5}$$

be a continuous piecewise linear approximation of $y_j(t)$. Substitute (5) into (2.3.9) and require the equation to hold at the mesh points $t = n\,\Delta t$. The result is the discrete equation of motion

$$\varepsilon_C Ci + \varepsilon_V V_i + U(s_i, y_i^n, n\,\Delta t) + \operatorname{erf}\left(\frac{y_i^n - y_i^{n-1}}{2\sqrt{\Delta t}}\right)$$
$$+ \sum_{m=0}^{n-2} \Delta s \sum_{-J}^{J\prime} (y_j^{m+1} - y_j^m) \int_0^1 \Theta(s_i - s_j, (n-m-\alpha)\,\Delta t)$$
$$\times K(y_i^n - y_j^{m+\alpha}, (n-m-\alpha)\,\Delta t)\,d\alpha = 0. \tag{6}$$

The weights can again be evaluated by Gaussian quadrature, the curvature and velocity are built with the derivative approximation D of the previous section, and consistency requires $J^2\,\Delta t \to \infty$ as $J \to \infty$, $\Delta t \to 0$.

Attention to several computational details can dramatically improve efficiency. First, note that the Θ-function values are fixed once we fix the time step, the mesh size, and the number of Gaussian quadrature points. Since they are used again and again, and each value is as expensive as half a dozen exponentials or trigonometric functions, a great increase in speed can be had by evaluating them at the beginning of the computation and storing them in an array. Next, it is very inexpensive to use

Newton's method for solving the nonlinear system (6) for y_j^n at time step n. This is because once we have the Θ-function values and exponentials necessary to evaluate (6), we can use them simultaneously to evaluate the Jacobian. The Θ-function values are the same in (6) and in its Jacobian, while the exponentials are simply related. This general situation—in which it costs very little to evaluate the Jacobian once the function itself has been evaluated—will recur in Section 4, though precomputation of Θ will not be possible then. And finally, it is also important to evaluate the error functions quickly and accurately. For this, we used Gautschi's algorithm [22], which relies on a power series expansion of erfce for small arguments and on Legendre's continued fraction for large arguments. The resulting values were spot-checked against 12-digit tables.

In our computations, we took symmetric initial conditions and used symmetry of the solution to compute only the side of the curve corresponding to $s \geqslant 0$, effectively cutting J in half. Since the cost of the method is

$$O(N^2J^2I) + O(NJ^3),$$

this reduces the total cost of the computation by a factor of 4.

2.6. *Numerical Results*

This section describes two numerical experiments with the method described in Section 2.5. In the first experiment, we compute the evolution of a cosine perturbation to a flat interface, compare the growth of the perturbation with that predicted by linear stability theory, and demonstrate the first-order convergence rate of the method by analyzing the variation of the solution with mesh size. In the second experiment, we study the evolution of an theta-function bump on a flat interface and again establish first-order convergence. In both cases, the solutions fail to converge after a certain time, when the gradients become too large. We see this as evidence of breakdown of a fundamental assumption of the periodic graph formulation; eventually, the interface is not a graph.

For the cosine perturbation, we took initial data $y_0(s) = g_0 \cos(ks)$ and initial temperature field

$$u_0(x, y) = u_0(y) + f(y)\cos(kx), \tag{1}$$

where

$$f(y) = \begin{cases} u_0' e^{-q'y} & y > 0, \\ u_0 e^{qy} & y < 0, \end{cases} \tag{2}$$

and $u_0(y)$ is given in (1.5.11). The forcing term is then

$$\begin{aligned} U(x, y, t) = U_0(y, t) &+ u_0' e^{-k^2 t} \cos(kx)\, F(y, t, q') \\ &+ u_0 e^{-k^2 t} \cos(kx)\, F(-y, t, q), \end{aligned}$$

where $U_0 = K * u_0$ and

$$F(y, t, q) = \frac{1}{2} e^{-y^2/4t} \operatorname{erfce}\left(\frac{2tq - y}{\sqrt{4t}}\right). \tag{3}$$

A moment's calculation shows that $\partial_y U$ blows up like $1/\sqrt{t}$ as $t \to 0$ unless the initial temperature field is continuous; $u_0 = u_0'$. Consistency of the initial interface and temperature perturbations requires (according to the calculation described in Section 1.5) that

$$u_0 = u_0' = -\tfrac{1}{2}(2\varepsilon_C k^2 - V) g_0 \tag{4}$$

if $\varepsilon_V = 0$. In this section, we take $\varepsilon_V = 0$ for simplicity. This is a more stringent test of our numerical method, because there is no velocity smoothing present.

First, we measured the convergence rate of the numerical method. We fixed the physical parameters

$$q = q' = V = 1, \qquad \varepsilon_C = 0.01, \qquad \varepsilon_V = 0, \qquad g_0 = 0.02, \qquad k = 4,$$

so that the cosine grows with the maximum exponent $y_1 = 2.43975 = \max_k y_1(k)$, and computed up to $t = 1.5$, with numerical parameters

$$J = 16, 32, 64, 128, \qquad N = 24, 48, 96, 192,$$

and $I = 4, 6, 8, 10$ Gaussian quadrature points per weight. The evolution is shown in Fig. 2, for the solution with $J = 64$; the final amplitude has increased by a factor of 50.

Since we do not know the exact solution, we estimate the error by studying the variation of the solution with successive halvings of the mesh size and time step. Table I displays the max–norm differences

$$\max_j y_{2j}^{2n}(2J) - y_j^n(J) \tag{5}$$

of the computed solution $y_j^n(J)$, as a function of time t and the number of points J. The halving of the differences as the mesh size is halved indicates first-order convergence;

$$y_j^n(J) = y(n\,\Delta t, j\,\Delta s) + \Delta s \cdot e(n\,\Delta t, j\,\Delta s) + O(\Delta s^2), \tag{6}$$

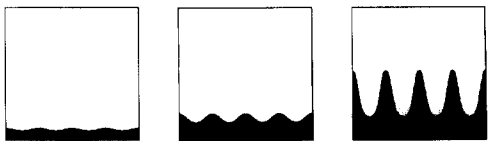

FIG. 2. Evolution of cosine graph. The physical parameters are $\varepsilon_C = 0.01$, $V = q = q' = 1$. The initial state has $g_0 = 0.02$, $k = 4$. The final state (computed with $J = 64$ and $N = 96$) has $T = 1.5$. The black region is ice, the white region is water.

TABLE I

Max–Norm Differences for Cosine Graph

t	32–16	64–32	128–64	(64/32)–(32/16)	(128/64)–(64–32)
0.125	0.00068	0.00040	0.00017	0.000115	0.000083
0.25	0.00230	0.00137	0.00062	0.000442	0.000180
0.375	0.00484	0.00298	0.00138	0.001114	0.000362
0.5	0.00869	0.00556	0.00264	0.002424	0.000708
0.625	0.01452	0.00971	0.00474	0.004896	0.001364
0.75	0.02330	0.01641	0.00827	0.009518	0.002624
0.875	0.03661	0.02742	0.01438	0.018235	0.005063
1.0	0.05704	0.04607	0.02538	0.035091	0.009816
1.125	0.08905	0.07900	0.04639	0.068942	0.021613
1.25	0.14039	0.14029	0.09015	0.140196	0.052824
1.375	0.22439	0.26210	0.19676	0.299807	0.131695
1.5	0.36218	0.52664	0.53837	0.691104	0.550101

Note. $V=1$, $\varepsilon_C=0.01$, $\varepsilon_V=0$, $g_0=0.02$, $k=4$, $q=q'=1$.

where $J\,\Delta t=1$, $y(t, s)$ is the exact solution, and e is an unknown smooth function of t and s. Hence we can build a second-order accurate solution by Richardson extrapolation [31]:

$$\tilde{y}_j^n = 2y_{2j}^{2n}(2J) - y_j^n(J) = y(n\,\Delta t, j\,\Delta s) + O(\Delta s^2). \tag{7}$$

The last two columns of Table I exhibit the maximum differences of the extrapolated solution $\tilde{y}$. There is some improvement in convergence, though the rate never quite reaches $O(\Delta t^2)$. But the final extrapolated solution is accurate to three digits all the way up to $t=1$, as far as we can tell by examining differences.

Next we compare the extrapolated results with the prediction

$$y(t, s) = Vt + g(t)\cos ks + O(g_0^2)$$

of linear stability theory. Here $g(t)$ is the solution of the linear stability equation (1.5.12). Since $g(t)$ is not an exponential, comparison with linear theory is complicated and requires comparison of the computed and exact functions $g(t)$ for a range of t, not just comparison of the computed and exact linear stability exponents γ_1. For simplicity, we took $\varepsilon_V=0$ ($\varepsilon_V\neq 0$ requires slightly more programming) and calculated the exact $g(t)$ by applying the second-order Runge–Kutta method [23] to the ordinary differential equation equivalent to (1.5.12). For the computed $g(t)$, we measured the amplitude

$$\tilde{g} = \tfrac{1}{2}(\max\,\tilde{y}_k - \min\,\tilde{y}_k) \tag{8}$$

of the extrapolated solution $\tilde{y}$. Figure 2 shows that an initial cosine wave remains a cosine with considerable fidelity. Clearly no other modes are being excited to any

significant extent, despite the nonlinearity of the problem. Thus the crude method (8) of amplitude fitting is reasonable.

Table II exhibits the results, for $k = 1$, 4, and 7. For each k, we tabulated the numerical and exact amplitudes $\tilde{g}$ and g, as well as the ratio between g and the prediction $g_0 e^{ty_1}$ of the classical linear stability theory reviewed in Section 1.4. Each entry in Table II is accurate to within two units in the last place, as estimated by measuring differences. The $k = 1$ column exhibits remarkably close agreement between $g \equiv \tilde{g}$, while the classical prediction is in error by as much as 25%. (Though the classical theory gets the right exponent, the amplitude is strongly affected by short-term transients neglected in the classical theory.) In this slow-growth situation, g behaves quite differently from an exponential.

In the $k = 4$ column, the entries increase much faster; the exponent y_1 here reaches its maximum over k. Thus linear theory cannot be expected to be accurate very long—and in fact it is good even to one digit only up to about $t = 1.25$. Our method breaks down then as well, to some extent; presumably the interface develops excessively large gradients, because it is about to stop being the graph of a single-valued function.

For $k = 7$, both theories agree well with the computed results, perhaps because the perturbation is decaying slowly and smoothly.

TABLE II

Comparison with Linear Stability Theory

	$k = 1$ $y_1 = 0.0955337$			$k = 4$ $y_1 = 2.43975$			$k = 7$ $y_1 = -0.360157$		
$16 \times t$	$\tilde{g}$	g	$g/g_0 e^{y_1 t}$	$\tilde{g}$	g	$g/g_0 e^{y_1 t}$	$\tilde{g}$	g	$g/g_0 e^{y_1 t}$
0	0.02000	0.02000	1.00	0.0200	0.0200	1.00	0.020	0.0200	1.00
1	0.02022	0.02022	0.95	0.0219	0.0219	0.94	0.019	0.0194	0.99
2	0.02067	0.02066	0.92	0.0253	0.0252	0.93	0.019	0.0189	0.99
3	0.02127	0.02126	0.89	0.0294	0.0293	0.93	0.019	0.0185	0.99
4	0.02200	0.02199	0.87	0.0343	0.0341	0.93	0.018	0.0181	0.99
5	0.02285	0.02285	0.85	0.0400	0.0397	0.93	0.018	0.0177	0.99
6	0.02382	0.02381	0.83	0.0467	0.0462	0.93	0.018	0.0173	0.99
7	0.02490	0.02490	0.82	0.0546	0.0539	0.93	0.017	0.0169	0.99
8	0.02610	0.02609	0.81	0.0638	0.0627	0.93	0.017	0.0165	0.99
10	0.0288	0.02881	0.79	0.087	0.0851	0.93	0.016	0.0158	0.99
12	0.0320	0.03200	0.78	0.12	0.1154	0.93	0.016	0.0151	0.99
14	0.0357	0.03569	0.77	0.17	0.1566	0.93	0.015	0.0144	0.99
16	0.0399	0.03992	0.77	0.23	0.2124	0.93	0.015	0.0138	0.99
18	0.0448	0.04474	0.76	0.3	0.288	0.93	0.014	0.0131	0.98
20	0.0503	0.5023	0.76	0.5	0.391	0.93	0.014	0.0126	0.98

Note. $\varepsilon_C = 0.01$, $\varepsilon_V = 0$, $V = 1$, $A = 0$, $g_0 = 0.02$.

[a] The extrapolated values for $k = 4$ and $t \geq 1.25$ are not converging swiftly enough to guarantee one good digit (g and $\tilde{g}$ are accurate within 2 units in the last digit shown).

In the second experiment, we computed the evolution of an initial Θ-function bump

$$y_0(s) = \frac{g_0}{\Theta(0, \delta)} \Theta(s, \delta) \tag{9}$$

on a flat interface. (The coefficient is chosen to make the maximum amplitude of the initial data equal to g_0.) An approximately consistent initial temperature field perturbation can be constructed via linear stability theory, for small g_0: Decompose Θ into its Fourier components, construct a consistent initial temperature field perturbation for each component by linear stability theory, as in the first experiment, and add up the results to get

$$u_0(x, y) = u_0(y) + e^{-q|y|}\left(\frac{V}{2} + \varepsilon_C \partial_x^2\right) y_0(x).$$

Here we assume $q = q'$, $\varepsilon_V = 0$, for simplicity. The forcing term is easily computed, because we chose Θ-function initial data,

$$U(x, y, t) = U_0(y, t) + (F(y, t, q) + F(-y, t, q)) \times \frac{g_0}{\Theta(0, \delta)}\left(\frac{V}{2} + \varepsilon_C \partial_x^2\right) \Theta(x, t + \delta).$$

F is given in (3). Figure 3 displays a sample result from a computation with

$$\delta = 0.05, \qquad g_0 = 0.02, \qquad q = q' = V = 1,$$

and an isotropic velocity-independent Gibbs–Thomson relation with $\varepsilon_C = 0.01$. We computed the solution with

$$J = 16, 32, 64, 128 \text{ points}$$

and

$$N = 24, 48, 96, 192 \text{ time steps}$$

up to time $t = 1.5$, using $I = 4$, 6, 8, and 10 Gaussian quadrature points. Again, the convergence was monotone and Richardson extrapolation gave a roughly second-

FIG. 3. Evolution of bump graph. The physical parameters are $\varepsilon_C = 0.01$, $\delta = 0.05$, $g_0 = 0.02$: The initial state is an almost invisible bump on a flat interface. We computed with $J = 64$ points and $N = 96$ time steps up to time $T = 1.5$.

order solution up to time $t = 1$. The full computation required 30 min of Cray X-MP CPU time, and we believe the final extrapolated solution to have three digit accuracy until $t = 1.5$.

Physically, there are two interesting features of the solution: First, the accuracy with which the flat ends of the interface move with the unperturbed velocity V. Thus a localized bump propagates slowly. Second, the depressions which form at each side of the central bump. These are not predicted by any physical argument known to us: they indicate that ice is melting immediately adjacent to the bump where water is freezing, a significant effect of curvature dependence.

3. Numerical Methods for General Periodic Fronts

3.1. *Introduction*

Section 3 contains a numerical method for computing an arclength parametrization of $\Gamma(t)$. This method does not require $\Gamma(t)$ to be the graph of a function. It takes advantage of a natural conserved quantity, the arclength deviation $Q = 1 - (x_s)^2 - (y_s)^2$ to eliminate x and y in favor of the new unknowns V and ϕ. Our numerical method conserves a natural analogue to Q, the scaled distance between one points and the next, by reconstructing x and y from V and ϕ in a special way. We calculate V from the integral equation and solve an evolution equation for the normal angle ϕ. A slight additional calculation is necessary to keep track of the arclength of one branch of the periodic curve.

The following algorithm may seem more natural: Put a set of marker points on the curve, evaluate the velocity at each point, and move each point along an approximation to the normal. This amounts to solving the equation $\mathbf{x}_t = V\nu$ for a non-arclength parametrization $\mathbf{x}$ of $\Gamma(t)$. However, Sethian [47] has described the difficulties in this approach when the velocity is a simple local function of curvature,

$$V = 1 - \varepsilon C.$$

(We cannot expect our much more complicated velocity to behave better.) Sethian observes that marker points tend to spread far apart in regions of larger curvature, where they are most needed to resolve sharp changes in the solution, and bunch up in flat areas, where they are least necessary. In the flat areas, a stability constraint of the usual kind $\Delta t/\Delta s \leqslant \text{const}$ then requires expensively small time steps. Another kind of spreading difficulty occurs, for example, when a bump is growing upward. On each side of the bump, the normal points sideways. Hence any algorithm which moves points only along the normal can only move a point on the side of the bump a short distance. Since points are not allowed to slide along the curve, they must inevitably spread out along each side. Sethian also describes why "rezoning" to keep points equidistant along the curve does not work; the interpolation required smooths the curve unconscionably.

3.2. *The ϕ Equation*

This section contains a derivation (based on [14]) of the evolution equation (2.6.9) for the normal angle ϕ on which our curve movement algorithm is based. Choose an arclength parametrization [9] $\mathbf{x} = \mathbf{x}(t, s)$ of an infinite interface $\Gamma(t)$, with s increasing as x increases, and with the special property that

$$\mathbf{x}_t(t, s=0) \cdot \mathbf{x}_s(t, s=0) = 0 \tag{1}$$

for each t. Thus we choose the point labelled by $s=0$ to move always along the normal to the curve. Given *any* arclength parametrization, we can shift the origin of arclength (by solving an ordinary differential equation) so that (1) is satisfied; hence this choice of parametrization involves no loss of generality. Recall that the normal velocity V is defined by [54]

$$V = \mathbf{x}_t \cdot \nu,$$

where

$$\nu = (-y_s, x_s)$$

is the unit normal to $\Gamma(t)$. This fixes only one component of the vector $\mathbf{x}_t$. The other component, $\mathbf{x}_t \cdot \tau$ (where $\tau = (x_s, y_s)$ is the tangent to $\Gamma(t)$), depends on the choice of parametrization. The special property (1) is enough to determine $\mathbf{x}_t \cdot \tau$, and therefore the parametrization, as it turns out. Indeed, τ is a unit vector, so $\partial_s \mathbf{x}_t \cdot \tau = \partial_t(\frac{1}{2}\tau \cdot \tau) = 0$, and thus

$$\partial_s(\mathbf{x}_t \cdot \tau) = \partial_s \mathbf{x}_t \cdot \tau + \mathbf{x}_t \cdot \partial_s \tau = -CV,$$

since $\partial_s \tau = -C\nu$ and $\mathbf{x}_t \cdot \nu = V$. Hence integration and (1) imply

$$\mathbf{x}_t \cdot \tau = -\int_0^s CV\, ds',$$

so $\mathbf{x}_t$ is given by

$$\mathbf{x}_t = V \cdot \nu - \int_0^s CV\, ds' \cdot \tau. \tag{2}$$

The first term moves points along the normal with velocity V; the second slides points along the curve to conserve arclength. Take components to get the "X/Y equations"

$$x_t + V y_s + x_s \int_0^s CV\, ds' = 0 \tag{3}$$

$$y_t - V x_s + y_s \int_0^s CV\, ds' = 0. \tag{4}$$

Here $C = y_s x_{ss} - x_s y_{ss}$.

The X/Y equations have—for any V—a natural conserved quantity, the arclength deviation (or *eikonal*)

$$Q = 1 - (x_s)^2 - (y_s)^2.$$

A short calculation shows that (3) and (4) imply a conservation law

$$\partial_t Q + \partial_s \left(Q \int_0^s CV \, ds' \right) = -CVQ. \tag{5}$$

This equation is linear in Q, so as long as CV is smooth, $Q = 0$ is the unique solution with initial values 0. Thus a parametrization which starts out as an exact arclength parametrization and evolves by the exact X/Y equations will remain an arclength parametrization. However, the nonzero right-hand side can cause exponential growth in a perturbation of Q. This is bad news for a numerical method based on the X/Y equations.

However, we can take advantage of the conservation of Q to reduce the number of degrees of freedom of our system from 3 (x, y, and V) to 2, and conserve Q automatically at the same time. We eliminate the constrained variables x and y, in favor of unconstrained variables V and ϕ. To do this, introduce the normal angle ϕ by

$$x_s = \cos \phi, \qquad y_s = -\sin \phi, \tag{6}$$

so that ϕ is the angle between the normal ν and the y-axis. Use (1), (3), and (4) to reconstruct x and y from ϕ and V by integration,

$$x(t, s) = x(0, 0) + \int_0^t \sin \phi(t', 0) \, V(t', 0) \, dt' + \int_0^s \cos \phi(t, s') \, ds' \tag{7}$$

$$y(t, s) = y(0, 0) + \int_0^t \cos \phi(t', 0) \, V(t', 0) \, dt' - \int_0^s \sin \phi(t, s') \, ds'. \tag{8}$$

The curvature C is the derivative of ϕ with respect to arclength:

$$C = -x_s y_{ss} + x_{ss} y_s = \partial_s \phi.$$

Finally, to construct an evolution equation for ϕ, differentiate (3) and (4) with respect to s, use (6), and take $\sin \phi$ times the first of the resulting equations plus $\cos \phi$ times the second. The result is the "ϕ equation"

$$\partial_t \phi + \partial_s V + \partial_s \phi \int_0^s V \, \partial_s \phi \, ds' = 0 \tag{9}$$

which will form the basis of our numerical method for moving curves.

EXAMPLE. Suppose $V=1$ is constant. Corresponding to the ill-posed Cauchy–Riemann initial value problem for the X/Y equations, the ϕ equation becomes Burgers' equation

$$\partial_t \phi + \partial_s(\tfrac{1}{2}\phi^2) = 0$$

if $\phi = 0$ at $s=0$, for example, if the curve is symmetric about $x=0$. Thus even in the seemingly simple case when V is constant, we cannot expect global solutions.

3.3. *Keeping Track of Arclength*

A slight additional complication, present in the case when $\Gamma(t)$ is periodic, is the need to keep track of arclength. Both the ϕ equation (3.2.9) and the integral equation (1.5.6) are to hold on the interval $-\infty < s < \infty$. As in Section 2.2, we want to reduce the problem to a finite interval by assuming that $\Gamma(t)$ is periodic. This means that

$$\begin{aligned} x(t, s+L(t)) &= x(t, s) + 2\pi \\ y(t, s+L(t)) &= y(t, s), \end{aligned} \tag{1}$$

where $L(t)$ is the length of one branch of the interface, unfortunately not known *a priori*. Then we can sum under the integral as in Section 2.2 to get the periodic integral equation

$$\varepsilon_C C + \varepsilon_V V + U(x, y, t) + \int_0^t \int_{-L/2}^{L/2} \Theta(x-x', t-t')\, K(y-y', t-t')\, V'\, ds'\, dt' = 0, \tag{2}$$

to hold for $-L/2 < s < L/2$. An easy calculation shows that $L(t)$ satisfies the differential equation

$$\partial_t L = \int_{-L/2}^{L/2} CV\, ds; \tag{3}$$

thus the integral equation (2), the ϕ equation (2.2.9), and (3) comprise a one-space-dimensional moving boundary problem. Fortunately, in one space dimension, moving boundaries can easily be removed by a stretching transformation which puts them into the coefficients of equations on a fixed domain. Thus put

$$g(t) = \frac{2\pi}{L(t)}, \qquad \sigma = g(t)s, \tag{4}$$

so that $-\pi \leqslant \sigma \leqslant \pi$, and let

$$\begin{aligned} \phi(t, s) &= \tilde{\phi}(t, \sigma) \\ V(t, s) &= g(t)\, \tilde{V}(t, \sigma). \end{aligned} \tag{5}$$

It follows from (3) that g satisfies

$$\partial_t g + g^3 \langle \tilde{V}\, \partial_\sigma \tilde{\phi} \rangle = 0, \tag{6}$$

where brackets denote the average

$$\langle f \rangle = \frac{1}{2\pi} \int_{-\pi}^{\pi} f(\sigma)\, d\sigma. \tag{7}$$

We now drop tildes, in order to simplify the notation.

3.4. *The Numerical Method*

First, we summarize the system of equations to be solved. The (rescaled) velocity

$$g(\varepsilon_C(\phi)\, \partial_s \phi + \varepsilon_V(\phi) V) + U(x, y, t)$$
$$+ \int_0^t \int_{-\pi}^{\pi} \Theta(x - x', t - t')\, K(y - y', t - t')\, V'\, ds'\, dt' = 0. \tag{1}$$

Here x and y are given by

$$x(t, s) = x(0, 0) + \int_0^t g(t') \sin \phi(t', 0)\, V(t', 0)\, dt'$$
$$+ \frac{1}{g(t)} \int_0^s \cos \phi(t, s')\, ds' \tag{2}$$

$$y(t, s) = y(0, 0) + \int_0^t g(t') \cos \phi(t', 0)\, V(t', 0)\, dt'$$
$$- \frac{1}{g(t)} \int_0^s \sin \phi(t, s')\, ds'. \tag{3}$$

Note that the actual normal velocity of the curve is gV, since we rescaled and dropped tildes. The curve is moved by calculating the normal angle ϕ and the arclength ratio g from

$$\frac{1}{g^2} \partial_t \phi + \partial_s V + \partial_s \phi \int_0^s (V\, \partial_s \phi - \langle V\, \partial_s \phi \rangle)\, ds' = 0 \tag{4}$$

$$\partial_t g + g^3 \langle V\, \partial_s \phi \rangle = 0. \tag{5}$$

Now we introduce continuous piecewise linear approximations in the time variable for the primary variables V, ϕ, and g, and require Eq. (1), (4), and (5) to hold at the mesh points $t = n\, \Delta t$. We use the asymptotic value

$$\int_{-\pi}^{\pi} \Theta(x - x', t - t')\, K(y - y', t - t')\, V'\, ds'$$
$$\sim K(\|\mathbf{x} - \mathbf{x}'\|, t - t')\, gV(t', s) \tag{6}$$

in the single layer potential at the top time level $t' > t - \Delta t$. The resulting semidiscrete equations are

$$g^n(\varepsilon_C(\phi^n)\,\partial_s\phi^n + \varepsilon_V(\phi^n)\,V^n) + U(x^n, y^n, n\,\Delta t) + \Delta t \sum_{m=0}^{n-2} \int_0^1 \int_{-\pi}^{\pi} \Theta(x^n - x^{m+\alpha}(s'), (n-m-\alpha)\,\Delta t) \times K(y^n - y^{m+\alpha}(s'), (n-m-\alpha)\,\Delta t)\, V^{m+\alpha}(s')\,ds'\,d\alpha + \Delta t \int_0^t K(\|\mathbf{x}^n - \mathbf{x}^{n-\alpha}\|, \alpha\,\Delta t)\, V^{n-\alpha} g^{n-\alpha}\,d\alpha = 0, \tag{7}$$

$$\left(\frac{1}{g^n}\right)^2 \frac{\phi^n - \phi^{n-1}}{\Delta t} + \partial_s V^n + \partial_s \phi^n \int_0^s (V^n(s')\,\partial_s\phi^n(s') - \langle V^n\,\partial_s\phi^n\rangle)\,ds' = 0, \tag{8}$$

and

$$\frac{g^n - g^{n-1}}{\Delta t} + (g^n)^3 \langle V^n\,\partial_s\phi^n\rangle = 0. \tag{9}$$

Here x and y are approximated by

$$x^n = x_0^0 + \Delta t \sum_{m=0}^{n-1}{}' V_0^m g^m \sin\phi_0^m + \frac{1}{g^n}\int_0^s \cos\phi^n(s)\,ds' \tag{10}$$

and

$$y^n = y_0^0 + \Delta t \sum_{m=0}^{n-1}{}' V_0^m g^m \cos\phi_0^m - \frac{1}{g^n}\int_0^s \sin\phi^n(s')\,ds'. \tag{11}$$

The subscript 0 on V and ϕ indicates evaluation at $s = 0$, $\|\mathbf{x}\|$ is the Euclidean norm of the vector $\mathbf{x}$, and the prime on the sum over m means that the first and last terms are to be halved.

The top weight in the semidiscrete integral equation (7) can be evaluated exactly in terms of the error function, as in Setion 2. A tedious calculation gives

$$\Delta t \int_0^1 K(\|\mathbf{x}^n - \mathbf{x}^{n-\alpha}\|, \alpha\,\Delta t)\, V^{n-\alpha} g^{n-\alpha}\,d\alpha = \frac{\sqrt{\Delta t}}{2}\,[W_{20}(z)\,g^n V^n + W_{11}(z) \times (g^{n-1}V^n + g^n V^{n-1}) + W_{02}(z)\,V^{n-1}g^{n-1}], \tag{12}$$

where $z = \|\mathbf{x}^n - \mathbf{x}^{n-1}\|/\sqrt{4\,\Delta t}$ and

$$W_{20}(z) = \operatorname{erf}(z)\left(\frac{1}{z} - \frac{1}{z^3} + \frac{3}{4z^5}\right) + \frac{e^{-z^2}}{\sqrt{\pi}}\left(\frac{1}{z^2} - \frac{3}{2z^4}\right)$$

$$W_{11}(z) = \operatorname{erf}(z)\left(\frac{1}{2z^3} - \frac{3}{4z^5}\right) + \frac{e^{-z^2}}{\sqrt{\pi}}\frac{3}{2z^4} \tag{13}$$

$$W_{02}(z) = \operatorname{erf}(z)\frac{3}{4z^5} - \frac{e^{-z^2}}{\sqrt{\pi}}\left(\frac{1}{z^2} + \frac{3}{2z^4}\right).$$

The other weights are computed by applying Gaussian quadrature in α and the trapezoidal rule in s, as in Section 2.

We could treat g differently: Introduce piecewise linear approximations only for V and ϕ, and solve the g equation exactly by transforming it into

$$\partial_t(1/g^2) - 2\langle V\,\partial_s\phi\rangle = 0,$$

which is linear in $1/g^2$. The resulting equation for g can be used in the integral equation and the reconstruction of x and y. However, we can no longer evaluate the top weight in the integral equation exactly, and eliminating g eliminates only one of a large number of discrete degrees of freedom, so we defer this approach to future work.

Next we discretize the curve. Let ϕ_j approximate $\phi(j\,\Delta s)$ and V_j approximate $V(j\,\Delta s)$, with $\Delta s = \pi/J$ and a positive integer J. Replace ∂_s with the discrete derivative D constructed in Section 2;

$$D\phi_j = \sum_{-J}^{J}{}' D_{jk}\phi_k,$$

where

$$D_{jk} = \frac{(-1)^{j-k}}{2}\cot\left(\frac{(j-k)\pi}{2J}\right), \qquad j \neq k,$$

$$D_{jk} = 0, \qquad j = k.$$

As we saw in Setion 2, this introduces a *consistency condition*

$$J^2\,\Delta t \to \infty \qquad \text{as} \quad J \to \infty,\ \Delta t \to 0. \tag{14}$$

We usually satisfy this condition by taking $J\,\Delta t = 1$.

The only new trick is in the construction of x and y from V and ϕ. The exact rescaled equations (1), (4), and (5) have the natural invariant

$$1 - g^2((x_s)^2 + (y_s)^2) = 0,$$

whose absolute constancy expresses conservation of arclength. We design our numerical method to conserve the analogous quantity

$$Q = 1 - \left(\frac{g}{\Delta s}\right)^2 ((x_j - x_{j-1})^2 + (y_j - y_{j-1})^2)$$

by using the special numerical integration rule

$$\begin{aligned} x_j - x_0 &= \frac{\Delta s}{g} \sum_1^j \cos \frac{1}{2}(\phi_i + \phi_{i+1}) \\ y_j - y_0 &= \frac{-\Delta s}{g} \sum_1^j \sin \frac{1}{2}(\phi_i + \phi_{i-1}) \end{aligned} \tag{15}$$

to compute x and y. Standard integration rules do not conserve Q, because they express $x_j - x_{j-1}$ as a sum of cosines rather than as the cosine of a sum.

Thus we have the discrete equations of motion

$$\begin{aligned} & g\varepsilon_C(\phi_i)\, D\phi_i + g\varepsilon_V(\phi_i) V_i + U(x_i, y_i, n\,\Delta t) \\ & \quad + \Delta t \sum_{m=0}^{n-2} \Delta s \sum_{-J}^{J\prime} \int_0^1 \Theta(x_i - x_k^{m+\alpha}, (n-m-\alpha)\,\Delta t) \\ & \quad \times K(y_i - y_k^{m+\alpha}, (n-m-\alpha)\,\Delta t)\, V_k^{m+\alpha}\, d\alpha \\ & \quad + \frac{\sqrt{\Delta t}}{2} [W_{20}(z_i)\, gV_i + W_{11}(z_i)(g^{n-1}V_i + gV_i^{n-1}) \\ & \quad + W_{02}(z_i)\, g^{n-1} V_i^{n-1}] = 0, \end{aligned} \tag{16}$$

$$\frac{1}{g^2} \frac{\phi_i - \phi_i^{n-1}}{\Delta t} + DV_i + D\phi_i\, \Delta s \sum_0^{i\prime} (V_i\, D\phi_i - \langle V\, D\phi \rangle) = 0, \tag{17}$$

$$\frac{g - g^{n-1}}{\Delta t} + g^3 \langle V\, D\phi \rangle = 0. \tag{18}$$

Here $z_i = \|\mathbf{x}_i - \mathbf{x}_i^{n-1}\|/\sqrt{4\Delta t}$, the integral over α is approximated by Gaussian quadrature, W_{ij} are given in (13),

$$\begin{aligned} x_i &= x_0^{n-1} + \frac{\Delta t}{2}(V_0\, g \sin\phi + V_0^{n-1} g^{n-1} \sin\phi^{n-1}) \\ &\quad + \frac{\Delta s}{g} \sum_{k=1}^{i} \cos \frac{1}{2}(\phi_k + \phi_{k-1}), \end{aligned} \tag{19}$$

$$\begin{aligned} y_i &= y_0^{n-1} + \frac{\Delta t}{2}(V_0\, g \cos\phi + V_0^{n-1} g^{n-1} \cos\phi^{n-1}) \\ &\quad - \frac{\Delta s}{g} \sum_{k=1}^{i} \sin \frac{1}{2}(\phi_k + \phi_{k-1}), \end{aligned} \tag{20}$$

unsuperscripted variables are evaluated at time level n, and

$$\langle V\, D\phi \rangle = \frac{\Delta s}{2\pi} \sum_{-J}^{J}{}' V_j\, D\phi_j.$$

We impose periodic boundary conditions $\phi_J = \phi_{-J}$, $V_J = V_{-J}$ and initial conditions for V, ϕ, and g.

The computational details are very like those mentioned in Section 2.5, except that precomputation of the Θ-function values is now impossible. However, the special feature which made Newton's method attractive is still present; it costs almost nothing to evaluate the Jacobian, once we have evaluated Eq. (16)–(18). Of course, the hand calculation involved in computing the matrix elements of the Jacobian is quite tedious and error-prone. But Newton's method performed well in the numerical experiments reported in the next section, requiring only five to six iterations to reduce the residual below 10^{-6} in Cray single precision (14 decimal digit) arithmetic. For $\varepsilon_V = 0$, Newton's method was occasionally (about one time in 1000) unable to reduce the residual below 10^{-6} even in 20 iterations; this is further evidence of the smoothing effect of velocity dependence.

3.5. *Numerical Results*

First, we validate the method with a convergence study. We compute a theta-function bump on a flat interface, with initial data

$$y(0, s) = \frac{g_0}{\Theta(0, \delta)}\, \Theta(s, \delta) \tag{1}$$

and a consistent exponential perturbation of the initial temperature field. The physical parameters are

$$\varepsilon_C = \varepsilon_V = 0.02, \qquad A = 0.5, \qquad k_A = 4,$$

so there is a 50% variation in curvature dependence from the y-axis to the x-axis, with growth up along the y-axis favored by the smaller value of ε_C there. Starting with the almost invisible bump ($\delta = 0.05$, $g_0 = 0.05$) shown in Fig. 4, the solution develops substantial gradients by time $t = 1.5$. We used J points and N steps, with

$$J = 10, 20, 40, 80, \qquad N = 15, 30, 60, 120,$$

and $I = 4, 6, 8, 10$ points for Gaussian integration of the weights. Table III exhibits the max-norm differences of the computed solution (x, y); on the finer meshes, a rough first-order convergence is evident. Furthermore, the error (measured by differencing) grows more or less linearly in time, indicating stability of the method.

Richardson extrapolation to second order produced three approximate solutions, with maximum differences shown in the last two columns of Table III. These decrease faster than the unextrapolated differences as the mesh becomes finer, but

TABLE III

Max-Norm Differences for Periodic Dendrite

t	20–10	40–20	80–40	10/20–20/40	20/40–40/80
0.2	0.0093	0.0030	0.0018	0.0040	0.0014
0.4	0.0127	0.0067	0.0041	0.0056	0.0023
0.6	0.0184	0.0133	0.0078	0.0099	0.0035
0.8	0.0303	0.0234	0.0133	0.0166	0.0051
1.0	0.0506	0.0384	0.0211	0.0262	0.0074

Note. $\varepsilon_C = 0.02$, $\varepsilon_V = 0.01$, $A = 0.5$, $k_A = 4$, $\delta = 0.05$, $g_0 = 0.05$, $q = q' = V = 1$.

do not quite attain second-order convergence. It is possible that the square-root singularity of K causes the convergence rate of the extrapolated solution to drop to $O(\Delta t^{3/2})$. Recall that our time discretization also appears to be of order $O(\Delta t^{3/2})$, perhaps for the same reason. At any rate, since the solution is of order unity, we have three good digits until $t = 1$.

Total computing time was 40 min on a Cray X-MP, over 90% of which was spent in evaluating the single layer potential. Thus the history-dependence of the velocity equation dominates the computational cost; this results in cost $O(N^2 J^2 I)$ to compute until time $T = N\Delta t$ with J points on the curve and I-point Gaussian quadrature.

A difficulty of the ϕ equation approach is that the periodicity of the curve cannot be maintained exactly. In the above computations, for example, x_J differed from π by several percent at $t = 1.5$. However, this difficulty is easily and naturally handled by rescaling; we simply divide each x_j by x_J. To keep the pictures properly scaled, we then must divide each y_j by x_J as well. We do not use this rescaling during the calculation, only when presenting graphical results.

We proceed next to the long-time computation of an anisotropic dendrite. The same initial interface, with physical parameters

$$\varepsilon_C = 0.04, \qquad \varepsilon_V = 0.02, \qquad A = 0.5, \qquad k_A = 4,$$

develops the structure shown in Fig. 5. We used $J = 40$ points and $N = 280$ time steps, computing until time $t = 7$ and using symmetry as usual to reduce the cost. In the last few pictures, we believe the beginning of a sidebranching instability to be appearing. It is cut off by impact on the neighboring dendrite before real

FIG. 4. Dendrite convergence study. Physical parameters: $\varepsilon_C = \varepsilon_V = 0.02$, $A = 0.5$, $k_A = 4$. Numerical parameters: $J = 40$, $N = 60$, $t = 0$, 0.75, 1.5.

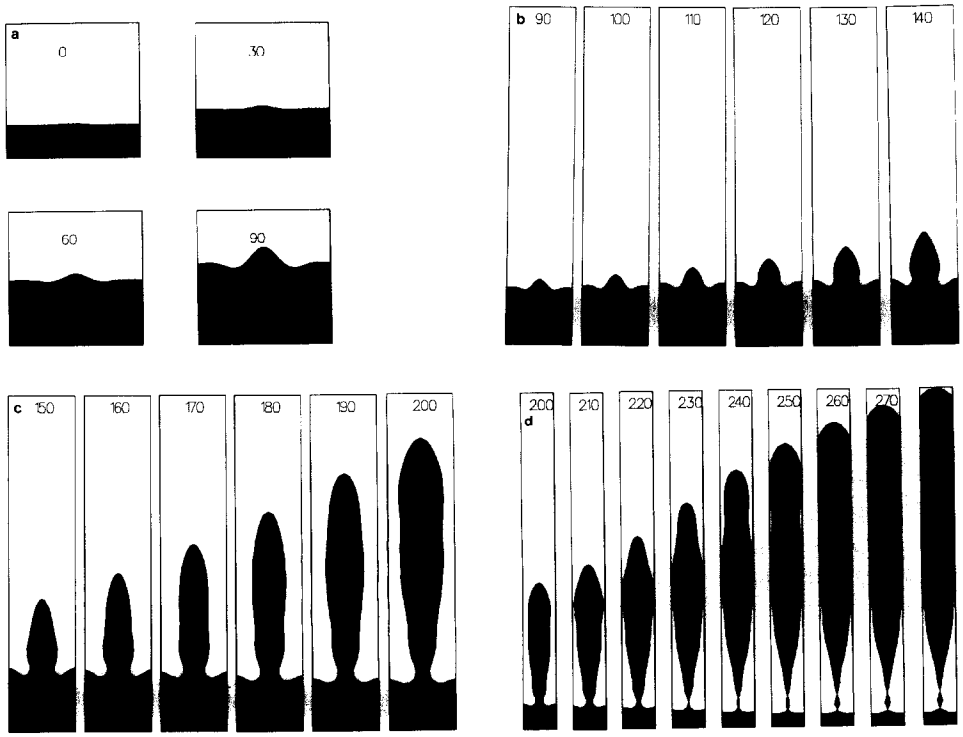

FIG. 5. (a) Evolution of an anisotropic dendrite. Physical parameters: $\varepsilon_C = 0.04$, $\varepsilon_V = 0.02$, $A = 0.5$, $k_A = 4$, $q = q' = V = 1$. Initial conditions: $\delta = 0.05$, $g_0 = 0.05$. The numerical parameters are $J = 40$, $N = 280$, $I = 10$, and we compute up to time $T = 7$. On this page, pictures are spaced 30 time steps apart, because the dendrite moves very slowly at first. Each figure is numbered on the top with the time step. (b) Now the development picks up speed, and pictures are taken 10 time steps apart. (c), (d) Evolution of an anisotropic dendrite continued.

sidebranch structure can develop, because of the periodicity of the calculation. Then the dendrites detach from their bases and the whole row of dendrites becomes a free-floating mass, separated from the ice below by a channel of water. (The last few pictures were rescaled to fit on the page.) In the region at the base, the curve sometimes crossed itself and formed a loop. When the sides of the curve left the channel available to them, they were modified for graphical purposes, by setting $x_j = \min(x_j, \pi)$.

We might see a true sidebranch structure develop, if we used a finer mesh and a narrower initial bump. The length scale of the dendrite should be determined by the initial conditions, so a narrower initial bump is equivalent to increasing the periodicity of the calculation. As the period (here equal to 2π) goes to infinity, we should recover an isolated dendrite. However, this would require more mesh points; then we would have to increase the time step as well, so this would make the computation extremely expensive.

An unexpected feature of the numerical calculation is the rapid growth of the condition number κ of the linear systems obtained by applying Newton's method to (3.4.16), (3.4.19) and (3.4.20), which we write as a system

$$F = \begin{pmatrix} F_V \\ F_\phi \\ F_g \end{pmatrix} = 0,$$

where $F_V = 0$ is the velocity equation and so forth. Then

$$\kappa = \operatorname{cond}(DF)_\infty = \|DF\|_\infty \|DF^{-1}\|_\infty,$$

where DF is the Jacobian of F and $\|A\|_\infty$ denotes the maximum row sum of the matrix A. Table IV exhibits κ as a function of t and J, in the computation of Fig. 5. The growth with J is not surprising, because one term in DF is essentially the spatial derivative D, which approximates an unbounded operator as $\Delta s \to 0$. The growth with t, on the other hand, is probably due to the breakdown of the ϕ equation formulation itself. The dendrite is clearly approaching its neighbor, and when they touch the parametrization can no longer be continuous. Instead, it must separate into two separate parts, each a continuous function on a separate interval. The ϕ equation, on the other hand, can make sense only if ϕ is no worse that a measurable function, so that $\cos\phi$ and $\sin\phi$ can exist. But then x and y are Lipschitz and hence continuous. Thus the ϕ equation formulation breaks down when the curve crosses itself.

The final set of figures (Fig. 6) show a dendrite with the same physical and numerical parameters as before, except that the Gibbs–Thomson relation has been made isotropic, with ε_C and ε_V equal to what were their minimum values in the previous calculation, $\varepsilon_C = 0.02$, $\varepsilon_V = 0.01$. Note the qualitatively different appearance. The dendrite now grows into an almost circular shape, and only then does it

TABLE IV

Growth in Condition Number for An Anisotropic Dendrite

t	$J=10$	$J=20$	$J=40$
1.0	1×10^2	2×10^2	3×10^2
2.0	1×10^2	2×10^2	4×10^2
3.0	3×10^2	7×10^2	3×10^3
4.0	4×10^3	2×10^4	6×10^4
5.0	3×10^4	7×10^4	3×10^5
6.0	6×10^4	2×10^5	6×10^5
7.0	1×10^5	2×10^5	1×10^6

Note. $\varepsilon_C = 0.04$, $\varepsilon_V = 0.02$, $A = 0.5$, $k_A = 4$, $\delta = 0.05$, $g_0 = 0.05$, $q = q' = V = 1$.

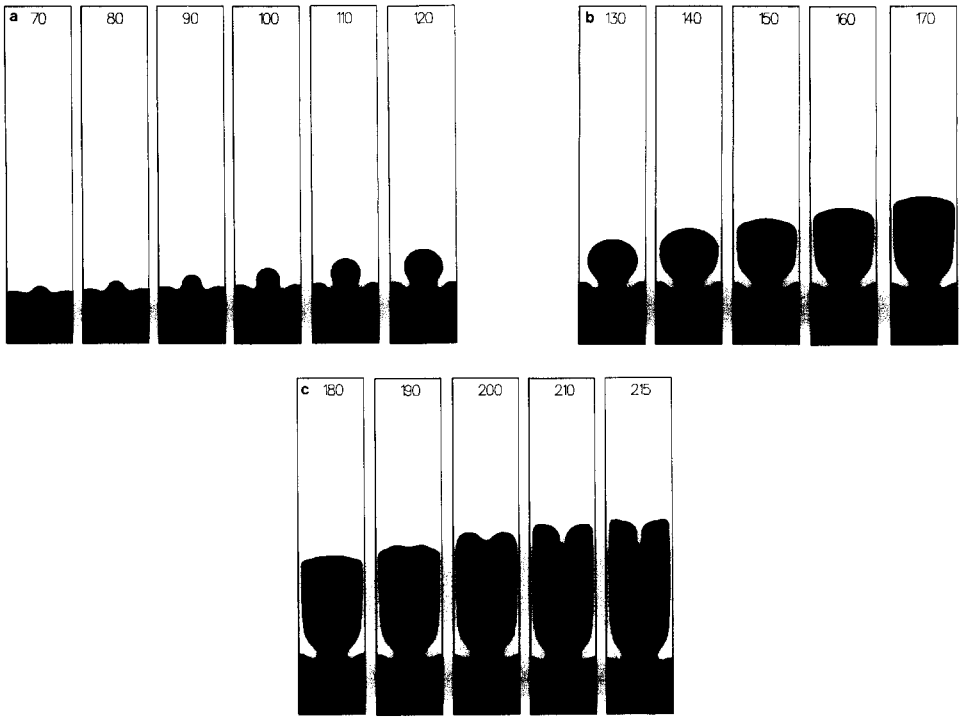

FIG. 6. (a) Evolution of an isotropic dendrite. Physical parameters: $\varepsilon_C = 0.02$, $\varepsilon_V = 0.01$, $A = 0$, $q = q' = V = 1$. Initial conditions: $\delta = 0.05$, $g_0 = 0.05$. The numerical parameters are $J = 40$, $N = 210$, $I = 10$, and we compute up to time $T = 5.25$. We omit the first few frames, because they are indistinguishable from those of Fig. 5. (b), (c) Evolution of an isotropic dendrite continued.

expand into a rectilinear shape filling the channel. A well-developed tip-splitting instability of the flat tip of the dendrite is then visible. Meiron [40] has exhibited very similar tip-splitting instabilities in an approximate steady state model. Nittmann and Stanley [43] also discuss connections between tip-splitting, sidebranching, and anisotropy, in a more general context. This computation failed at about $t = 5.4$, due to exponent overflow. We believe this happened because 40 points is no longer sufficient to capture the structure at the center of the split, where a singularity seems to be forming. With only 40 points, smoothness cannot be maintained. Of course, it is also possible that the true solution itself blows up, in the sense that a real cusp develops at the split. Table V displays the condition number of the Jacobian as a function of t and J.

Each dendrite computation required about 2 h of CPU time on a Cray X-MP. Gaussian elimination with partial pivoting and iterative improvement solved the linear systems well (in Cray single-precision 14-digit arithmetic) despite the large condition numbers, and Newton's method took less than five steps to reduce the residual below 10^{-6} at each time step.

TABLE V

Growth in Condition Number of an Isotropic Dendrite

t	$J=10$	$J=20$	$J=40$
1.0	8×10^{1}	2×10^{2}	3×10^{2}
2.0	1×10^{2}	2×10^{2}	5×10^{2}
3.0	4×10^{2}	2×10^{3}	8×10^{3}
4.0	5×10^{3}	2×10^{4}	6×10^{4}
5.0	2×10^{4}	8×10^{4}	3×10^{5}
6.0	2×10^{4}	[a]	[a]
7.0	3×10^{4}	[a]	[a]

Note. $\varepsilon_C = 0.04$, $\varepsilon_V = 0.02$, $A = 0$, $\delta = 0.05$, $g_0 = 0.05$, $q = q' = V = 1$.

[a] The calculation blew up at $t = 5.4$ for $J = 20$ and $t = 5.3$ for $J = 40$; the condition number at blowup was in each case 9×10^{5}.

4. Discussion and Conclusions

We have presented a numerical method for solving the supercooled Stefan problem with an anisotropic curvature- and velocity-dependent temperature boundary condition imposed on the moving boundary. We simplify the problem by eliminating the temperature field; thus only the moving boundary need be computed. We compute the normal velocity by solving a singular integral equation on the moving boundary and move the curve by solving an evolution equation for the normal angle. An additional ordinary differential equation is solved for the arclength.

Our numerical method turns out to be stable, first-order accurate, and fairly expensive—though the high cost may be unavoidable given the intrinsic difficulty of the problem. The method costs

$$O(N^2J^2I) + O(NJ^3)$$

arithmetic operations to compute up to a fixed time $T = N\,\Delta t$, with time step Δt, J points on the curve, I Gaussian quadrature points per weight, and $J\,\Delta t = 1$. The first term, due to the history-dependence of the single layer potential, dominates in practice.

The method exhibits an $O(\Delta t)$ convergence rate, which compares favorably with the $O(\Delta t^{1/2})$ or worse of weak solution methods for *classical* Stefan problems (i.e., without curvature-dependence or supercooling). Furthermore, this method avoids "grid effects" which contaminate weak solution methods and prevent Richardson

extrapolation to higher order. Grid effects are avoided by computing only the moving boundary and eliminating the temperature field.

Our numerical results agree with the linear stability theory based on the integral equation formulation. Previous authors have not obtained agreement between numerical results and the classical theory because their numerical results are contaminated by grid effects and because the classical theory is incorrect in the short-time regime, which is the only regime where linear theory can be expected to be accurate. For longer time spans, the classical theory is asymptotically correct, but linearized theory breaks down, because perturbations grow.

Our velocity calculation algorithm is constructed by studying the special case when the boundary is a graph. As far as the velocity is concerned, this situation already presents all the difficulties: The singularity of the kernel, the consistency condition for numerical integration over the curve, and the discretization of curvature can all be understood in this special case.

The general case, when the boundary is not the graph of a single-valued function, requires a reformulation of the general problem of how to move a curve with a given curvature-dependent velocity. Methods which move points only along the normal fail: Points along the side of a bump spread apart, causing loss of accuracy, whereas points in other areas move too close together, requiring expensively small time steps to maintain numerical stability.

Thus we turn to a different formulation of curve movement, based on the "ϕ equation." This formulation takes V and ϕ as primary variables, reconstructing x and y only when needed. Thus arclength is automatically conserved in the exact equation. The numerical method then requires a special integration rule to evaluate x and y, in order to preserve the numerical equivalent of arclength. Taking V and ϕ as primary variables amounts to computing time and space derivatives of the prametrization, and therefore ensures smoothness of the resulting curve.

We worked with a spatially periodic curve, to simplify the boundary conditions, but this is not at all necessary. Our curve movement algorithm is quite general: it applies without change to any periodic curve movement problem, and appropriate fictitious boundary conditions would permit its extension to almost any curve.

The velocity calculation algorithm seems quite special to the Stefan problem; it depends on being able to reduce the equations determining the normal velocity to equations on the interface. Nevertheless, this approach naturally extends to solve a number of other problems, for example, the supercooled Stefan problem with the heat equation $\partial_t u = \Delta u$ replaced by the steady state heat equation (in a moving frame), $\Delta u + V \partial_y u = 0$, in each phase. This approximation assumes that the temperature field relaxes quickly compared to the movement of the interface. The steady state heat equation makes the problem much easier to solve numerically, because the single layer potential is no longer history-dependent. Thus this modification of the problem would eliminate the need to store previous locations of the interface and reduce the cost of the method to

$$O(NJ) + O(NJ^3);$$

the second term, the cost of Gaussian elimination, would presumably dominate in this case. Even so, we could expect a great decrease in computational cost. A difficulty in this formulation, however, is the choice of the constant V. If the tip of a dendrite were known to move with constant velocity, the tip velocity would be a natural choice of V. Unfortunately, this is not known, so V is an adjustable parameter in the theory.

Another interesting problem is to compute an infinite dendrite; much recent work [34, 40] has been devoted to this, but many important questions of pattern formation and velocity selection remain unanswered. The extension of our method to this case should be straightforward, requiring only fictitious boundary conditions to truncate the infinite curve.

ACKNOWLEDGMENTS

I thank my thesis advisor, Alexandre Chorin, for his encouragement and advice. I have also benefited from conversations with Ole Hald, Matania Ben-Artzi, and James Sethian.

REFERENCES

1. R. ALEXANDER, P. MANSELLI, AND K. MILLER, *Rend. Accad. Naz. Lincei (Rome) Ser. VIII* **67**, 1–2 (1979).
2. M. BEN AMAR AND Y. POMEAU, *Europhys. Lett.* **2**, 3307 (1986).
3. E. DI BENEDETTO AND A. FRIEDMAN, *Trans. Amer. Math. Soc.* **282**, 183 (1984).
4. A. E. BERGER, H. BREZIS, AND J. C. W. ROGERS, *RAIRO Anal. Num.* **13**, 297 (1979).
5. L. A. CAFFARELLI, *Comm. Partial Differential Equations* **5**, 427 (1980).
6. G. CAGINALP, *Superlattices Microstruct.* **3**, 595 (1987).
7. G. CAGINALP AND J. T. LIN, *IMA J. Appl. Math.* **39**, 51 (1987).
8. J. W. CAHN AND J. E. HILLIARD, *J. Chem. Phys.* **28**, 258 (1958).
9. M. P. DO CARMO, *Differential Geometry of Curves and Surfaces* (Prentice–Hall, Englewood Cliffs, NJ, 1976).
10. A. J. CHORIN, *J. Comput. Phys.* **57**, 472 (1985).
11. P. COLLET AND J.-P. ECKMANN, *Commun. Math. Phys.* **107**, 39 (1986).
12. C. W. CRYER, "The Interrelation Between Moving Boundary Problems and Free Boundary Problems," in *Moving Boundary Problems*, edited by D. G. Wilson, A. D. Solomon, and P. T. Boggs (Academic Press, New York, 1978).
13. P. J. DAVIS AND P. RABINOWITZ. *Methods of Numerical Integration* (Academic Press, New York, 1975).
14. J. DUCHON AND R. ROBERT, *Ann. Inst. Henri Poincaré* **1**, 361 (1984).
15. G. DUVAUT, *C.R. Acad. Sci. Paris Ser. A* **276**, 1461 (1973).
16. H. DYM AND H. P. MCKEAN, *Fourier Series and Integrals* (Academic Press, New York, 1972).
17. E. B. FABES AND N. M. RIVIERE, in *Proceedings of the American Mathematical Society Conference on Singular Integrals* (Amer. Math. Soc., Providence, RI, 1979), p. 179.
18. G. J. FIX, "Numerical Methods for Alloy Solidification Problems, in "Moving Boundary Problems," edited by D. G. Wilson, A. D. Solomon, and P. T. Boggs (Academic Press, New York, 1978).
19. G. J. FIX, "Numerical Simulation of Free Boundary Problems Using Phase Field Methods," in *The Mathematics of Finite Elements and Applications IV (Uxbridge*, 1981) (Academic Press, London/New York, 1982), p. 265.

20. A. FRIEDMAN, *Trans. Amer. Math. Soc.* **133**, 51 (1968).
21. O. FROSTMAN, Thesis, Lund, 1935 (unpublished).
22. W. GAUTSCHI, *ACM Trans. Math. Software* **5**, 466 (1979).
23. C. W. GEAR, *Numerical Initial Value Problems in Ordinary Differential Equations* (Prentice-Hall, Englewood Cliffs, NJ, 1971).
24. M. GEVREY, *Œuvres* (Centre National de la Recherche Scientifique, Paris, 1970).
25. J. GLIMM, O. MCBRYAN, R. MENIKOFF, AND D. H. SHARP, *SIAM J. Sci. Statist. Comput.* **7**, 230 (1986).
26. M. E. GURTIN, *Arch. Rat. Mech. Anal.* **100**, 275 (1988).
27. J. M. HILL, *One-dimensional Stefan Problems: An Introduction* (Wiley, New York, 1987).
28. P. J. VAN DER HOUWEN AND H. J. TE RIELE, *Math. Comput.* **45**, 439 (1985).
29. S. C. HUANG AND M. E. GLICKSMAN, *Acta Metall.* **29**, 717 (1981).
30. J. M. HYMAN, *Physica D* **12**, 396 (1984).
31. E. ISAACSON AND H. B. KELLER, *Analysis of Numerical Methods* (Wiley, New York, 1966).
32. F. JOHN, *Partial Differential Equations* (Springer-Verlag, New York, 1982).
33. D. A. KESSLER, J. KOPLIK, AND H. LEVINE, *Phys. Rev. A* **33**, 3352 (1986).
34. D. A. KESSLER AND H. LEVINE, *Phys. Rev. Lett.* **57**, 3069 (1986).
35. D. KINDERLEHRER AND G. STAMPACCHIA, *An Introduction to Variational Inequalities and Their Applications* (Academic Press, New York, 1982).
36. J. S. LANGER, *Rev. Mod. Phys.* **52**, 1 (1980).
37. J. S. LANGER, *Physica A* **140**, 44 (1986).
38. J. L. LAVOIE, T. J. OSLER, AND R. TREMBLAY, *SIAM Rev.* **18** 240 (1976).
39. E. A. MCINTYRE, JR., *Math. Comput.* **46**, 71 (1986).
40. D. I. MEIRON, *Physica D* **23**, 329 (1986).
41. G. H. MEYER, "The numerical solution of multidimensional Stefan problems—A survey," in *Moving Boundary Problems*, edited by D. G. Wilson, A. D. Solomon, and P. T. Boggs (Academic Press, New York, 1978).
42. W. W. MULLINS AND R. F. SEKERKA, *J. Appl. Phys.* **35**, 444 (1964).
43. J. NITTMANN AND H. E. STANLEY, *Nature* **321**, 663 (1986).
44. V. K. PINUS AND P. L. TAYLOR, *Phys. Rev. B* **33**, 8697 (1986).
45. L. I. RUBENSTEIN, *The Stefan Problem* (Amer. Math. Soc. Mathematical Monographs, Providence, RI, 1971).
46. Y. SAITO, G. GOLDBECK-WOOD, AND H. MULLER-KRUMBHAAR, *Phys. Scr.* **T19**, 327 (1987).
47. J. A. SETHIAN, *Commun. Math. Phys.* **101**, 487 (1985).
48. J. B. SMITH, *J. Comput. Phys.* **39**, 112 (1981).
49. J. STRAIN, *SIAM J. Appl. Math.*, in press.
50. J. STRAIN, *Physica D* **30**, 297 (1988).
51. J. STRAIN, Ph.D. thesis, University of California, Berkeley, and Lawrence Berkeley Laboratory Report No. LBL-25698, 1988 (unpublished).
52. J. M. SULLIVAN, D. R. LYNCH, AND K. O'NEILL, *J. Comput. Phys.* **69**, 81 (1987).
53. F. TREVES, *Introduction to Pseudo-Differential and Fourier Integral Operators* (Plenum, New York, 1980).
54. C. TRUESDELL AND R. A. TOUPIN, The Classical Field Theories, in *Handbuch der Physik III*/1 (ed. S. Flügge) (Springer-Verlag, Berlin, 1960).
55. C. VERDI AND A. VISINTIN, *Boll. Un. Mat. Ital. B* (7) **1**, 795 (1987).
56. A. VISINTIN, *IMA J. Appl. Math.* **35**, 233 (1985).
57. G. B. WHITHAM, *Linear and Nonlinear Waves* (Wiley, New York, 1978).
58. D. G. WILSON, A. D. SOLOMON, P. T. BOGGS (Eds.), *Moving Boundary Problems* (Academic Press, New York, 1978).
59. D. J. WOLLKIND AND R. D. NOTESTINE, *IMA J. Appl. Math.* **27**, 85 (1981).